IMPROVING THE EFFICIENCY AND PERFORMANCE OF A THERMOACOUSTIC LASER POWERED BY PULSED THERMAL RADIATION

by

Mohammed Albonaeem

A thesis submitted to the faculty of
The University of Utah
in partial fulfillment of the requirements for the degree of

Master of Science

Department of Mechanical Engineering

The University of Utah

December 2015

The University of Utah Graduate School

STATEMENT OF THESIS APPROVAL

The thesis of **Mohammed Albonaeem**

has been approved by the following supervisory committee members:

Kuan Chen	, Chair	**8/12/2015**
		Date Approved
Meredith M. Metzger	, Member	**8/12 /2015**
		Date Approved
Kent S. Udell	, Member	**8/12 /2015**
		Date Approved

and by **Timothy A. Ameel** , Chair/Dean of

the Department/College/School of **Mechanical Engineering**

and by David B. Kieda, Dean of The Graduate School.

ABSTRACT

This study involved conducting experiments to obtain a clear, high-amplitude acoustic signal through the use of a new design of thermoacoustic converter. The thermoacoustic converter used photoacoustic effects to generate sound from solar energy within frequency range 200-3000 Hertz (Hz). The amplitude range of the thermoacoustic signal in this experiment was 86.5 decibel (dB) to 98.3 dB.

The thermoacoustic energy conversion system consisted of a lens and a chopper wheel to create air pressure fluctuations inside a thermoacoustic converter attached to a small microphone. Though a high-amplitude signal was produced, the signal was contaminated with noise. Over the course of the study, new electric cables, insulation materials, and a shock mount were added to the converter and microphone to reduce noise. In later experiments, light- and heat-reducing window films were used to control the amount of solar radiation entering the converter to ensure production of a sine wave in frequencies 200-3000 Hz.

The author performed Fast Fourier Transform (FFT) and time-domain analysis on the signal using LabVIEW and MATLAB software. Analysis revealed that: the noise reduction techniques (shock mount device, insulation materials, and new set of electric connection cables) were effective in significantly reducing the background noise; the new thermoacoustic converter design was effective in creating a loud, clear sound; and the geometry of the thermoacoustic converter was critical for increasing the amplitude of the

sound. After implementing noise reduction techniques, noise amplitude was reduced by 93%. The amplitude of the signal was improved by 83% for frequencies 200–3000 Hz but only 60% for frequencies 1000–3000 Hz. In particular, it was found that the reduction of vibration through use of the shock mount device improved the thermoacoustic (TA) laser signals considerably. With noise reduction techniques, the relationship between the amplitude and frequency of the thermoacoustic signal decreased nearly linearly within frequency range of 1000–3000 Hz.

Finally, calibration procedures were conducted to convert Volt units to dB units, measure the loudness of the signal at specific frequencies, and compare it with previous research.

TABLE OF CONTENTS

LIST OF TABLES

Tables

ACKNOWLEDGEMENTS

I would like to express my sincere thanks to Dr. Kuan Chen for his patient guidance throughout my research. He was like a father to me as I worked on this project. His advice and insight about my work, and the hours he spent proofreading and helping me draft this thesis, are what allowed me to finish in an effective and efficient manner. I am also grateful for the contributions from my committee members; without their help, this study would not have been completed.

This work would not have been possible without the support of a number of other people. I would like to thank my family. They are always in my heart, particularly my brother, who encouraged me to be a better person and engineer. My friends at the University of Utah were instrumental in helping me complete my project, especially my coworker and friend Aowabin Rahman, who helped me through the uncertainty analysis, Faisal Fathiel, who designed the thermoacoustic converter that I used, and Tony Roehrig, who helped me solve the electrical problems in the study. I am also grateful to Alfred Mowdood, University of Utah librarian, who helped me find the best resources for my research and taught me how to cite sources accurately.

Finally, I would like to acknowledge the generous support from the National Research Foundation of Korea.

CHAPTER 1

INTRODUCTION

Thermoacoustics is a branch of science that involves the study of both acoustics and thermodynamics [1]. The interaction between thermodynamics (which is the study of the behavior of heat) and acoustics (which is the study of the behavior of sound waves), leads us to study both in order to understand thermoacoustic phenomena [2], or the way heat creates sound.

When gas particles are heated, they release kinetic energy, causing an increase in temperature and randomness (entropy variation). The creation of sound from heat depends on two conditions. First, the pressure oscillation must travel through a medium which has inertia and elasticity. For example, when sound propagates through air, an air particle tends to transfer momentum to adjacent air particles. When reaction force is applied to this particle, it returns to its original position. These properties of the medium are necessary to create pressure oscillations. Second, producing sound depends on the ability of the source to vibrate and then generate an air pressure disturbance [2–6]. In other words, as Albers stated, sound is the feeling in a human ear that is created by a compression wave [6]. From the view of physics, sound needs two components: the reference of sound and the properties of the medium through which sound is transmitted [5]. Generally, a sound wave is the change of velocity and pressure of air molecules in

space in relation to temperature change [7, 8].

This scientific knowledge about heat and the creation of sound has been combined in the dual field of thermoacoustics. Bryon Higgins (1777) was the first scientist to observe acoustic oscillation in a large, open-ended tube containing a hydrogen flame [9]. In 1850, Sondhass confirmed Higgins' work by using a glass tube experiment (with only one end open) to produce sound through heating the tube [9]. Later, in 1859, Rijka did the same experiment as Sondhass, but with two differences: Rijka's experiment was conducted with porous material inside a tube which had two ends exposed [9]. Details of these three experiments are shown in Figure 1.1 (more details about these experiments will be discussed in Chapter 2).

In 1880, Alexander Graham Bell used photoacoustic phenomena to invent a wireless phone, which he called the photo phone. Bell noticed that using mirrors to reflect the sun into a selenium cell, which was linked to a conventional telephone device, generated a sound wave. Changing the position of the beam of sunlight changed the sound that was produced [10]. The historical context that informs this project is further developed in Chapter 2.

Acoustic energy has a wide application of uses in such different fields as petrochemical, medical, biomedical, industrial, and mining [8, 11]. For example, the Primasonics company has used 60–240 Hz acoustic cleaners to remove particulate build-up that occurs during the flow processes of specific equipment such as boilers, electrostatic precipitators, and air classifiers. Particulate matter accumulates in the pipes and ductwork of these mechanical systems. Instead of shutting the machinery down and sending human workers through hazardous conditions to manually clean them, the sound

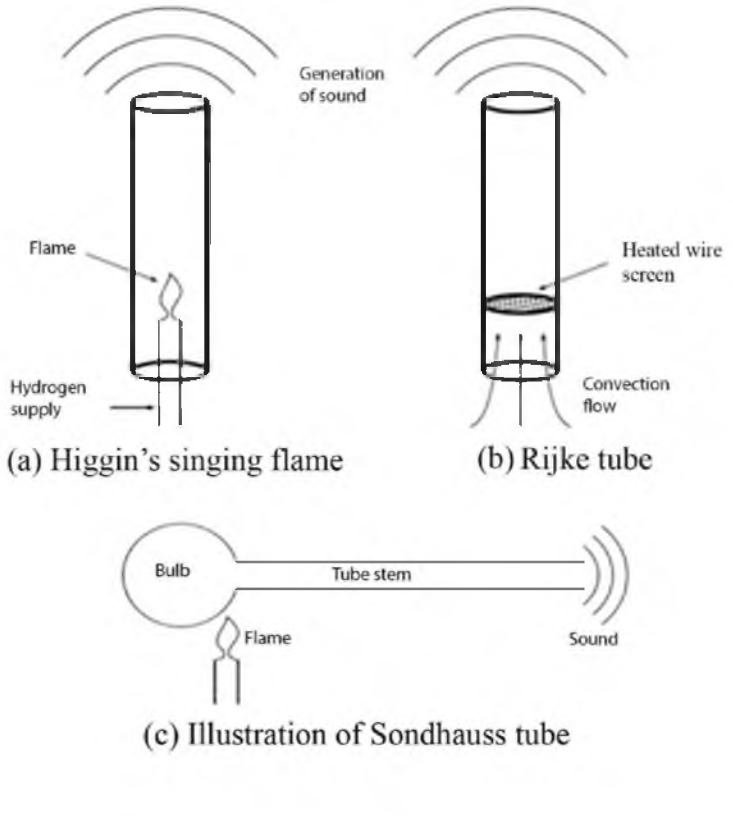

Figure 1.1 The three fundamental experiments for thermoacoustics [12].

waves from acoustical cleaners can be used to remove the material safely and efficiently [13]. Acoustic cleaners are also used to clean cargo ship holds, silos and hoppers, turbines, and filters. As a way to reduce costly and hazardous manual maintenance, particularly on inaccessible parts of the equipment, acoustic cleaners are environmentally friendly, effectively clear particulate build-up, increase operation efficiency, reduce corrosion and damage to the equipment, avoid accidents associated with manual cleaning, and reduce equipment downtime [13]. Use of acoustic energy in the medical field ranges from noninvasive medical procedures such as kidney stone shattering to the cleaning and sterilization of medical equipment [11]. The acoustic signals generated in this study are

specifically useful for cleaning [8, 11]. With slight increase in chopper wheel diameter and motor speed, the frequency of generated sound can be easily increased to 10 kHz or above. Such high-frequency sound waves have many uses. For example, sound waves in the frequency range 100–8000 Hz can be used in the medical field for the diagnosis and treatment of early-childhood hearing loss [14]. Sound waves higher than 16 kHz can be used in sono-assisted food processing and preservation, including extraction, drying, crystallization, filtration, oxidation, and meat tenderization [15].

In recent years, because of the wide range of applications for acoustics, the low environmental impact of the energy generated, and the development of modern simulation tools, researchers' interest in thermoacoustics has grown. Most of the work in thermoacoustics has been done using thermoacoustic (TA) engines and lasers. The research in this thesis used a lens and a chopper wheel to create acoustic waves from solar radiation. This TA laser uses sunlight to create sound directly in an environmentally friendly way. TA lasers also have few moving parts, so mechanical failure is low. While this study involves the use of a motor to spin the chopper wheel, the converter itself has no moving parts and uses no energy other than solar radiation.

To create a contribution to this burgeoning field of thermoacoustics, and further develop the possibility of obtaining environmentally-friendly acoustic energy in an inexpensive, sustainable way, the author conducted an experiment grounded and informed by literature in this field. This study focused on using pulsed thermal radiation and a thermoacoustic laser to produce sound. The first purpose of the experiment was to examine the amplitude of thermoacoustic signals created through the use of a new thermoacoustic converter. The converter was designed by Faisal Fathiel, a graduate

student at the University of Utah. The new thermoacoustic converter was designed to create stronger acoustic signals than what has been produced by converters used in previous research. Design modifications of the converter to facilitate enhanced sound production include a smaller diameter for the opening and a shorter air column. Unlike earlier designs, the converter is also very airtight. The smaller dimensions of this converter have a direct effect on the amplitude of the sound produced by the converter. The design specifications of the converter will be discussed in detail in Chapter 3.

The second purpose of this experiment was to obtain a clearer signal by reducing sources of noise that were contaminating the thermoacoustic signal. The author improved the thermoacoustic signal by using new noise reduction techniques that involved adding a shock mount device, insulation materials, and new set of electric connection cables. This combination reduced noise from various outside sources and improved the clarity of the sound produced. Details on these noise reduction techniques are presented in Chapter 3.

The experiment was done outdoors in direct sunlight in order to examine a wide frequency range (200Hz–3000Hz). To enhance the production of sound by the converter, special care was taken to find the best focusing point for the chopper wheel, correctly align the converter with the chopper wheel, and then keep them in alignment as the position of the sun changed. Moreover, the author initiated a step in the experiment procedure to allow the converter to cool. This cooling period (approximately 3 minutes) reduced the temperature of the converter and augmented the performance of the converter.

The observed results of this study indicate that the acoustic signals generated from solar radiation during the outdoor experiment are much higher than those obtained by

previous researchers. In fact, the amplitude of the thermoacoustic signal within the low-frequency range (200 to 860 Hz) was equal to 98.3 dB, which indicates a very loud sound generated inside the airtight TA converter. However, the signals within this range were beyond the detection thresholds of the microphone used, resulting in a truncated wave in the time domain plots. Initially, low-frequency data were excluded from this study. However, new experiments were run using solar window films to reduce the solar radiation entering the converter. After applying the films, an approximate sine wave was achieved in the low-frequency range.

Results also showed that the noise reduction techniques utilized through the experiment were effective in decreasing contaminating noise and obtaining a pure thermoacoustic signal. With noise reduced from the signal, and films to control the amount of solar radiation entering the converter, the experiments also revealed that the relationship between frequency and amplitude is nearly linear at high frequencies. It was found that increasing the frequency of the chopper wheel reduced the amplitude of the thermoacoustic signal. This is because the absorption time of the pulsed solar radiation decreased when increasing the speed of the chopper wheel. The cooling time of the porous material inside the converter between solar radiation pulses is also important to increasing the temperature differences between the air inside the TA converter and the porous material in order to generate a strong acoustic signal.

The significance of this experiment lies in the new design of the converter, the addition of noise reduction techniques, the utilization of a period of time to allow the converter to cool down, and the use of window films to control the intensity of the solar radiation entering the converter for nondistorted microphone signals.

CHAPTER 2

LITERATURE REVIEW

This thesis study focused on TA lasers powered by pulsed thermal radiation. This chapter presents the conversation that inspired this experiment, specifically the discovery and development of photoacoustic phenomena, in order to show the possible important aspects of thermoacoustic phenomena.

2.1 Early Experimentation With Thermoacoustics

In 1777, Brian Higgins was the first inventor to convert heat to acoustic energy by using a hydrogen flame, which was called the "singing flame," inside a tube with two ends open. This flame caused changes in the air density in the tube which translated into sound oscillation [16, 17]. Later in the eighteenth century, glass blowers accidently produced a sound by heating a glass tube [18]. Karl Sondhass, in 1850, built upon Higgins' work by experimenting with a glass tube to produce sound through heating [19]. He noticed that the dimensions of the glass tube affected the frequency of the sound created by the tube [4]. Sondhass used a tube with one end open to generate sound [4]. Sondhass clarified that the air particles moved to the hot end of the tube when applying heat to the closed end. The kinetic energy of the air particles increased when photons were absorbed by the air particles, causing the pressure to increase at the closed end. As

these particles changed their temperature with the wall of the tube, they accelerated toward the low-pressure area at the cool end of the tube [3, 20]. As the air particles moved out of the tube, it caused a sound. The cycle repeated itself between the atmosphere and the air particles inside the Sondhass tube [3]. Many tests were conducted by Sondhass in order to identify the proper dimensions of the tube for this experiment. The dimensions of the tube played an important role in his experiment to diagnose the factors that affect the frequency of sound [4, 19]. Sondhass' experiments showed that the temperature gradient of the air particles inside the tube produced sound [19]. Sondhass also identified that the intensity of the sound generated inside the tube depended on the temperature of the flame [4].

Later, in 1859, Pieter Rijka did an experiment similar to Sondhass'. However, Rijka's experiment was conducted with a fine mesh inside a vertical tube with two exposed ends [12, 19]. Heating the mesh generated a sound wave [19]. Rijka recognized that the location of the mesh in the tube affected the tone of the sound and he clarified that the mesh should be placed one quarter of the way up from the bottom of the tube [4].

In 1868, Gustav Robert Kirchhoff conducted the first theoretical calculation in his thermoacoustic study to evaluate the transfer of heat between a duct wall and the air in the duct. Kirchhoff derived an equation for the thermal attenuation of sound. He also studied the viscous effect that occurs in a thin, boundary layer [9, 21]. His experiments drew attention to the role of the boundary layer of air in the interaction of sound waves and heat. These theoretical works helped advance the progress toward understanding thermoacoustic phenomena.

2.2 Alexander Graham Bell's Photophone

In 1880, a wireless phone, called the photophone, was invented by Alexander Graham Bell. This phone relied on photoacoustic phenomena to create sound [10]. Bell's photophone contained two major parts: a transmitter and a receiver [22, 23]. The transmitter was composed of a flexible mirror reflecting the solar flux. The function of the transmitter was to reflect the incident light beam toward the receiver [10, 22]. The receiver was a conventional telephone device linked to a selenium cell. The transmitter's mirror reflected sunlight onto the selenium cell and thus generated a sound wave (see Figure 2.1) [10, 8]. With this invention, Bell had invented a device for signaling and communicating by using the properties of sound transfer through a light beam [23] and, along the way, identified that the angle that the sun hits the mirror is critical to the process of producing sound waves [10, 23]. According to Bell's analysis, the range of this signal depended on the time of the day and the brightness of the sun [22]. This experiment established the fundamentals of wireless telephony [22].

Later on, Bell developed his idea of generating sound from the sun by using a new method which chopped the solar flux through two rotating perforated wheels (see Figure 2.2) [24]. His new method consisted of a mirror, two wheels, and a parabolic receiver [24]. In this device, light reflected off a mirror through the two perforated wheels (the first wheel rotated around its axis while the other remained constant). The perforation of the wheels chopped the solar flux into pulses of light. These light pulses were received by a parabolic glass that contained a sensitive material (lampblack). The heating of the lampblack caused contraction and expansion of the air particles in the parabolic space, resulting in the generation of sound into the attached ear tube [24].

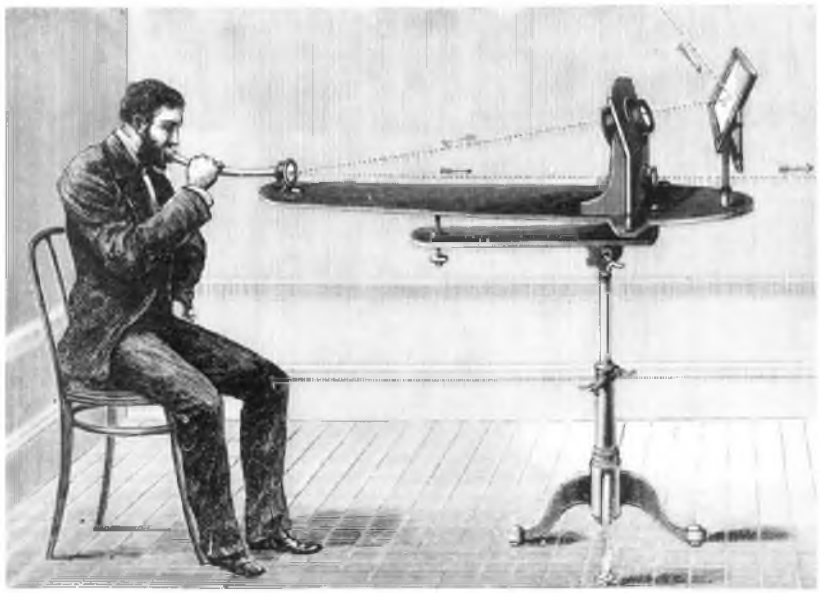

Figure 2.1 Alexander Graham Bell's photo phone [25].

Figure 2.2 Alexander Graham Bell's experiment to create sound by using chopper wheels [26].

Bell's invention opened the doors to John Tyndall and Wilhelm Roentgen. In 1881, they verified that photoacoustic phenomena were valid not only in gases but also in liquids [8]. Later, in 1896, Lord Rayleigh clarified Sondhass' work qualitatively as stated below:

> If heat be given to the air at the moment of great condensation, or be taken from it at the moment of the greatest rarefaction, the vibration is encouraged. On the other hand, if heat be given at the moment of greatest rarefaction, or abstracted at the moment of the greatest condensation, the vibration is discouraged [27].

2.3 Twentieth- and Twenty-First Century Advancements in the Field

The twentieth century saw increased development of thermoacoustics. Additional research on the study of sound vibration was conducted by K.W. Taconis. In 1949, he discovered that when immersing a closed, gas-filled tube in liquid nitrogen, chilling it to cryogenic temperatures, the temperature gradient inside the tube triggered a sound [3].

Robert Leroy Carter, in 1962, discovered that adding a bundle of glass tubes inside Sondhass' tube increased the performance of the sound production [4]. Carter's experiment further established that adding a stacked material inside the tube played an important role in generating an improved thermoacoustic signal inside the tube [4].

In 1973, an experiment was conducted by Parker. He observed sound signals generated from a window cell which led him to carry out a theoretical analysis on photo acoustic signals [28, 29]. Shortly after that, in 1976, Rosencwaig and Gersho proved that periodic heat radiation on a porous sample produced acoustic waves, demonstrating that heat transfer between a solid material and a boundary layer of air generates sound waves [8]. They used a cylinder cell with a specific diameter and length and a microphone to measure the sound generated through photoacoustic phenomena. Their work established

that the pressure variation of the sample is critical in generating acoustic waves, and that the signal depends on the transportation of the pressure variation to the microphone through a medium [28, 29].

In the 1980s, thermoacoustic research began diverging along two paths: continuous heat or pulsed radiation. Among the notable researchers in continuous heat source-based thermoacoustics is Hatzawa who, in 2004, proposed the creation of a heat engine that uses waste heat—such as heat from cars. Advanced study was conducted by Luke Zoontjens et al. using the car's own hot exhaust to run the air conditioning system inside the car through the use of thermoacoustic devices. Instead of refrigerant in a vapor compression system, thermoacoustic phenomena used waste heat to cool the car [30, 31]. In recent years, Symko, Chen, and other researchers at the University of Utah have investigated high-frequency TA lasers and TA laser pairs. Electrical heaters were used in their experiments to produce sound [11, 18].

Anil Kolhe Sanket clarified in 2012 that changing the geometry parameters of the stack-in-a-tube TA laser could vary the sound waves produced. He deduced that increasing the length of the tube produced low-frequency signals [32]. Surathu Rohit's 2013 work built on Sanket's findings and confirmed that the dimensions of the tube had an effect on the frequency of the signal and that the TA laser outputs were out of phase by 180° when the crossing angle of a TA laser pair was small [19].

In the area of thermoacoustics using pulsed radiation, Markus Sigrist established in 1986 that an acoustic wave generates through incident pulsed heat radiating on a medium (air). The interaction between solid materials at a high temperature and a boundary layer of air played an important role in his study. He clarified that

thermoacoustic phenomena were generated because of heat transfer between the solid materials and the boundary layer [8, 33].

In 2013, Aowabin Rahman established that acoustic waves can be created by using thermal radiation hitting a porous material inside a thermoacoustic converter. He found that the relation between the amplitude of the sound and the magnitude of the radiation is nearly linear. Along with that, during his experiments, the opening diameter of the TA converter, the air volume within, and the length of the porous material inside affected the amplitude of the TA signal. The amplitude decreased with an increase in the air volume. Further, he established that the temperature of the converter also affects the amplitude of the sound produced. Finally, Rahman's research began the work of compiling microphone calibration plots [8].

The research in this thesis builds on Rahman's results in several ways. Based on Rahman's observation that a greater air volume in the converter leads to lower sound amplitudes, a new converter was designed to contain a smaller air volume to obtain higher amplitude signals. Since Rahman's converter was not very airtight, it could not produce high-amplitude sounds. The converter in this research was more airtight and the resulting amplitude was higher than what Rahman had achieved. Rahman's signal was also contaminated with significant noises. This research worked to eliminate those noises by applying noise reduction techniques. Not only that, but with Rahman's findings about the effect of the temperature of the converter, the new experiment utilized a cooling period for the converter.

CHAPTER 3

TA CONVERTER DESIGN AND IMPROVEMENTS

3.1 An Introduction to the Theory

The experiment in this thesis is similar in concept to Bell's study in converting solar energy to sound energy. As described before, Bell clarified that the sound generated in his experiment depended on specific conditions: the brightness of the sun and the time of the day [22]. This thesis project began during the summer of 2014 (May–July) with experiments to obtain sound waves of high-amplitude by using a more airtight design for the thermoacoustic converter.

This study relies on the thermoacoustic phenomena associated with the thin layer of air that lies adjacent to a solid material. An understanding of the behavior of this penetration depth of surface temperature fluctuation helps to improve thermoacoustic phenomena. A small penetration depth of surface temperature fluctuation of air, close to a solid material, is responsible for creating thermoacoustic phenomena through the interaction of temperature differences and heat between the penetration depth of surface temperature fluctuation and the solid material [34]. As the solid material is heated and cooled, heat is transferred into or out of the penetration depth of surface temperature fluctuation, which responds by expanding or contracting.

In 2014, Rahman established that a larger opening diameter for the TA converter

causes an increase in the heated area of the porous material (steel wool) which leads to an increase in the temperature fluctuation between the steel wool and the air surrounding the steel wool inside the TA converter at low frequencies. However, a larger opening diameter may also reduce the cooling of the air inside the TA converter in the high-frequency range, impeding temperature fluctuations in the thermal boundary layer. Thus there should be an optimal opening diameter for maximum sound amplitude.

The length and diameter of the cylindrical air volume of the TA converter also has an important role in generating a loud sound inside the TA converter. The dimensions of the air volume inside the TA converter are responsible for increasing or decreasing the amplitude of the TA signal. This is due to the inverse relationship of the pressure fluctuation with the air volume of the TA converter. The length of the porous material and the position of the microphone inside the TA converter both affect the air volume of the TA converter [8].

The quality of the confinement of air inside the converter is also important to the strength of the pressure wave created. Rahman's research with TA converters resulted in a low amplitude TA signal due to the longer air column inside the converter and the lack of a good airtight seal due, in part, to the lack of an O-ring. In order to increase sound amplitudes at high frequencies, a new converter would need to be designed with an optimal opening diameter, a shorter air column length, and a better airtight seal.

3.2 Functions of the Components of the TA Converter

The new converter was designed by Faisal Fathiel, a University of Utah graduate student. Aside from an aluminum body held together by screws, the converter has the

following major components.

1. Steel wool: a porous material that absorbs the pulsed solar radiation to contribute to the creation of sound inside the TA converter. This wool is very fine. The interaction between the steel wool filaments and the air inside the TA converter generates pressure fluctuations when periodic solar radiation striking the converter causes the temperatures of the steel wool and the air to fluctuate [8].
2. Silicon O-ring: an o-shaped material used to seal the circular groove inside the TA converter to make it airtight when interfacing with the glass cover. The diameter of this O-ring is 4.81 cm (OD) and 3.74 cm (ID). This silicon O-ring works perfectly in a wide temperature range (-65–450° F) [35].
3. Glass cover: used to cover all the components that are mentioned above and create the confined medium condition required for better sound production inside the TA converter when the solar radiation penetrates through it.

The aluminum body of the converter was machined with grooves of different diameters on the left end. The function of the different grooves was to make a secure bed for the steel wool, the O-ring, and the glass cover. See Figure 3.1.

3.3 Assembly of the Converter

In order to measure the sound wave created by the converter, a microphone of sufficient sensitivity must be used in the experiment. The careful placement of the microphone within the converter is crucial to the success of the experiment.

Setting the microphone inside the converter efficiently involved the following

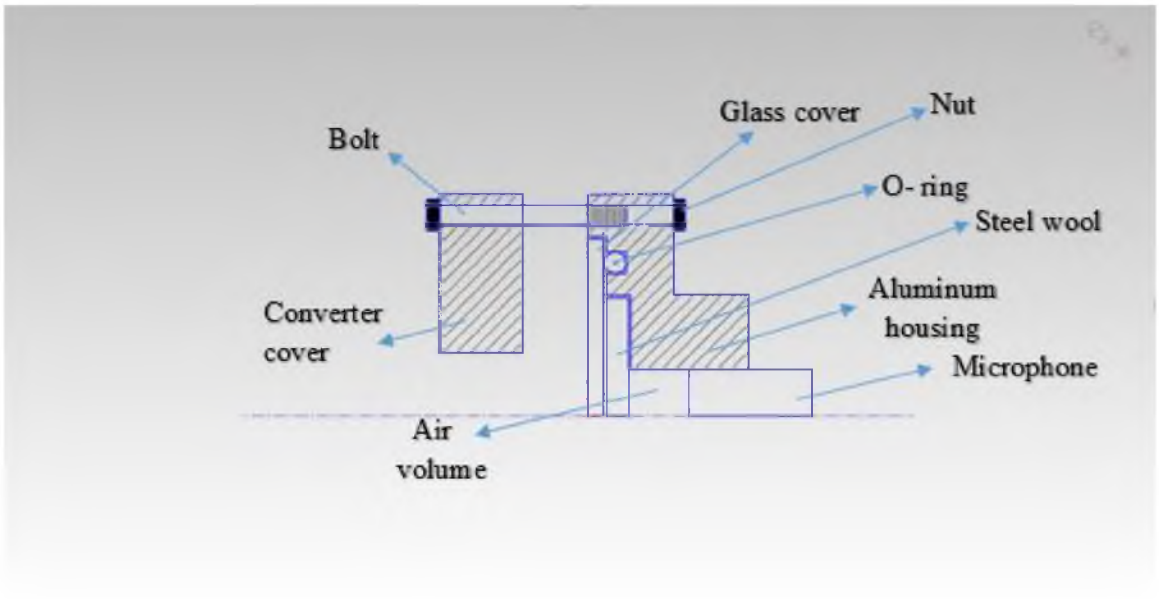

Figure 3.1 Assembly of the TA converter.

steps:

- Cut the steel wool and fit it inside the converter.
- Position the silicon ring inside the converter and place the glass cover over it.
- Place the steel cover over the converter and tighten it together with the converter base by using screws.
- Use Allen (hex) key to tighten the screws and ensure the converter is air tight.
- Place the microphone at the back of the converter and seal it with hot glue.
- Using a clamp to hold the converter, place the converter about 2 cm behind the chopper wheel.

During data analysis for the experiment conducted in summer, 2014, it became apparent that the sound signal was affected by noise from various internal and external sources (cart vibration, wind, generator, chopper wheel rotation, and electronic noise).

Various noise reduction techniques were introduced to the experiment, with insulation materials being added first and then a shock absorber and new electronic connections.

3.4 Insulation Materials and Shock Mount Device

An insulation process was examined in this study to investigate the influence of insulation materials on the sound signal after applying the insulation materials to the converter and the microphone. Insulation materials are described in terms of their ability to resist air flow and their absorbency of pressure fluctuations [36]. For instance, when air particles move between fibers, friction (resistance in fibrous materials) is generated between the air particles and the fiber. The absorption of the insulation materials determines what amount of the energy from the air particles (kinetic energy) is absorbed [36]. In particular, the amplitude of the sound wave decreased after adding insulation materials because the sound wave faced resistance from the fibrous materials of the insulation [37]. Vibration studies conducted by the American Society for Testing and Materials (ASTM) have determined that fibrous insulation works very efficiently at high-frequency ranges (greater than 1000 Hz) and is less effective at low-frequency ranges (less than 250 Hz) [5]. Because the experiment in this study was looking to reduce the amplitude of the noise signal mainly in the high-frequency range, porous insulation materials were chosen for this study.

The insulation materials chosen for this experiment were composed of the following main components:

1. Fiberglass (multipurpose, unfaced insulation on a continuous roll): a material that is used in different engineering applications because of its unique

properties. Fiberglass properties are: light weight; good shape; inexpensive; simple to install, split, and cut; and very soft [38]. Fiberglass is a porous material that is used to absorb sound energy when sound passes through it. The expansion and compression of air particles faces friction when interacting with the fiber filaments and this friction causes sound attenuation [39]. Fiberglass was wrapped around the microphone to control the sound and temperature in this experiment.

2. Reflective tape: reflective foil tape is made of aluminum to create a reflective surface that strengthens the insulation process. This tape is characterized by an adhesive layer, radiant barrier, and flexibility [38]. It was wrapped firmly around the microphone.
3. Insulation duct tape: used to increase the insulation and to seal any gap that existed after wrapping the fiberglass and reflective tape around the microphone. This duct tape is an adhesive that is sticky and very durable [38].

In addition to the use of the above insulation materials, a microphone shock mount was used to reduce the vibration (high isolation) of the microphone. The specifications of the microphone shock mount are [40]:

- A locking knob used to change the angle of the shock mount.
- Fits a microphone with 48 to 54 mm diameter [40]. The diameter of the converter and microphone placed at the back of it after including all insulation materials on it was 50 mm diameter.
- Foam to hold the microphone and protect it.

The process of adding the insulation includes wrapping fiberglass, reflective tape,

and insulation duct tape around the converter and the microphone. Glue was then added to all of the insulation materials, specifically on the part of the converter where the insulation met the converter in order to prevent the insulation materials from sliding away from the converter. At the end of the insulation process the bracket of the shock mount was squeezed to open it up in order to slide the microphone in. This bracket holds the microphone tightly. Figures 3.2–3.7 illustrate the insulation and shock mount process.

3.5 Enhancement of the Electric Circuit

The sound signal of this study became more stable after replacing the old connectors with durable, high-quality, efficient, and easily installed connectors [41]. The rotation of the chopper wheel at a high frequency (>1000 Hz) caused the experiment cart to vibrate wildly which, in turn, vibrated the electronic cable, resulting in unwanted noise. The new connectors minimized the fluctuation of the signal's amplitude.

The connectors were manufactured by the Q-See company, model number QS50B. The new connectors' package included

- 50 ft. /15 m extension cable.
- Bayonet Neill-Concelman (BNC) connection.
- Two BNC female connectors (female to female coupler) which are very simple to plug in and install.
- One male to female power connector.

This package is advertised as able to provide a strong signal despite any movements made during the process [41, 42]. Furthermore, in order to illustrate that the new cables provide a strong signal in comparison to old cables, an indoor experiment was

Figure 3.2 The first step of the insulation process: adding fiberglass around the microphone.

Figure 3.3 The second step of the insulation process: adding reflective aluminum tape around the microphone.

Figure 3.4 The third step of the insulation process: adding insulation duct tape around the microphone.

Figure 3.5 The fourth step of the insulation process: adding glue around the microphone to cover the area between the converter and the insulation so that the insulation sticks to the converter without a gap.

Figure 3.6 The shock mount used in this experiment.

Figure 3.7 The fifth step of the insulation process:
inserting the microphone into the shock mount.

performed composed of two speakers, a microphone connected to a data card, and a computer. Moreover, LabVIEW and Tone generator software were used in this experiment. The amplitude of background noise, after using new cables, was reduced about 18% in comparison to old cables. In addition, the amplitude of the sound signal of the new cable at 1000 Hz was improved by 7% when compared to old cables.

The noise reduction techniques also involved using a new RCA connector (jacks) and a new Dimart BNC male (manufactured by the Test Cable Company) connected to the data acquisition card through port A0.

Finally, all electric circuits for this experiment were improved by checking and evaluating the safety of the circuit and ensuring that voltage, ampere, and phase for all connected devices and cables were electrically compatible. The old cord that connected the transformer to the converter was replaced with a new cord and receptacle (male and female plug, 20 A 250 V) and the cord that connected the converter to the electric motor was also replaced with a new cord and grounded receptacle. This receptacle and cord performed efficiently during the high summer temperatures. The receptacle is 20 A, 250 V, and the cord is 12 AWG (American Wire Gauge-Conductor), made of rubber, 10 ft. long with four conductors. The maximum limit of this cord is 600 V and it is suitable for high-temperature environments [38].

CHAPTER 4

EXPERIMENT SETUP AND PROCEDURES

The goal of this chapter is to show in detail the experiment setup and the procedure used in this study. This experiment involved a sequence of investigations on how to obtain a high-amplitude, pure signal by minimizing external noise. A new design of TA converter was used in order to obtain high-amplitude sound waves during an outdoor experiment. A shock absorber, insulation materials, and a new set of connection cables were added to the converter in this experiment in order to minimize the amplitude of the disturbing vibrations. The experiment setup can be seen in Figure 4.1.

4.1 The Major Components of the TA Energy Conversion System

This system was developed and used in Rahman's thesis study:

1. Lens: this device converged the solar radiation. The dimensions of this lens were 73 cm diameter and 89 cm focal length. The lens used in the experiment was made of plastic. In the experiment, the device was mounted on a cart.
2. Chopper wheel: this device was made of steel, with a diameter of 47 cm, and 60 holes (each hole had a 1 cm diameter) on the perimeter. The radial distance from the center of each hole to the center of the chopper wheel was 19 cm.
3. Thermoacoustic (TA) converter: this device converted sunlight into

Figure 4.1 The equipment on the cart and the focusing point on the chopper wheel.

soundwaves. The TA converter was critical in this experiment in order to obtain higher amplitude waves compared to previous work. This device was placed about 2 cm behind the chopper wheel and fixed on the cart by use of a holder. The device included fine steel wool, a silicon O-ring, and a glass cover. The dimensions of this converter are presented in Appendix B. A microphone was placed inside the TA converter and sealed with glue to the back of the converter. The microphone had an intermediate level of filtration to remove electronic noise. The microphone contained two RCA (Radio Corporation America) connectors (sockets) to carry the sound signal.

The features of this microphone were [43]:

- High sensitivity (-54 dB) [as related in a phone call to the company].
- Preamplifier (power adaptor) (12 V) to increase the output voltage.
- Small size with 5 mm outside diameter.

Due to its high sensitivity, preamplifier, and small size, this model microphone is typically used for video security and spy purposes. Moreover, during the indoor tests, the amplitude of background noise that was measured by the microphone during the indoor experiment varied from one microphone to another by anywhere from 10–20% even though the background noise was almost the same inside the lab. To ensure consistency, the author used one microphone for all data collection.

4. Data acquisition card: this device was used to collect and translate the microphone signals to digital signals and send them to the computer. Then the signals were visualized and analyzed using LabVIEW and MATLAB

software. The model number of this card was NI-DAQ 6009 by the National Instruments Company. According to the National Instruments Company, 48000 samples per second is the maximum sampling rate in each channel of the card [44]. For further specifications, see Appendix A.

5. Electric motor: this device was mounted on the cart to rotate the chopper wheel. The model number was 2nKY4 from Dayton Company.
6. Solar pyranometer: this device was used to measure the solar heat flux. Model number SP-110, manufactured by the Apogee Company.
7. Alignment surface: this device was designed by Rahman to maximize the solar flux by using the shadow principle. The wooden alignment surface had a nail screwed into it. For maximum solar flux, the nail should have a minimum shadow.
8. Speed controller: this device contained a knob to control the speed of the electric motor. The device was manufactured by the Freenic Mini Company, model number FRN002.
9. Transformer: this device was manufactured by the Variac Company and it converts the voltage from 120 V to 220 V. The device was set to 220 V.
10. Generator: a generator was used to provide power for all the electrical devices used in this experiment. The model number of this portable generator was 67560 from the Chicago Electric Company.
11. Cart: Most of the equipment for this experiment, specifically the lens, chopper wheel, electric motor, TA converter, holder, pyranometer, and alignment surface, were mounted on this cart. The TA converter, the chopper wheel, and

the lens were mounted in an inclined way on the cart to collect maximum solar flux into the TA converter. The cart contains a level (scissor jack) to change the position of the inclined plane depending on the movement of the sun during the day.

4.2 The Experimental Procedure

The experimental procedure was outlined as follows:

- Take the cart to the parking area at the NW corner of MEB.
- Connect the laptop power cable, transformer, and the preamplifier cable of the microphone to the multi-plug.
- Connect the data acquisition card to the microphone through the A0 port.
- Connect the data acquisition card to the laptop using the USB port.
- Check the gasoline level and oil level in the generator and check if the generator is set on cold chock.
- After checking that all the equipment is connected to the multi-plug on the generator, check electronic connection, and then turn the generator on (warm chock).
- Set the volume of the computer to 20% and the volume of the speakers at maximum (so as to avoid dangerous levels of sound).
- Run the LabVIEW software (signal express 2009), time domain data should appear on the computer screen.
- Set the transformer on 220 V.
- Adjust the alignment of TA system. The shadow of the nail on the alignment

surface should be minimal and both the solar pyranometer and the nail should be perpendicular to the flat alignment surface. The lens was mounted on the same inclined platform that aims at the sun. The chopper wheel and the TA converter should be in the same alignment position as the lens to obtain maximum solar flux into the TA converter. In order to obtain the strongest solar flux, it is necessary to manually adjust the position and inclination angle of the TA system from time to time (see Figures 4.2 and 4.3).

- Place the TA converter about 2 cm behind the chopper wheel. For each outdoor experiment, it takes 1–3 minutes to determine the focusing point of the solar flux. This is done by placing a cover with a small, circular hole in the center over the lens, adjusting the position of the TA converter based on the focused sun image on the chopper wheel, and then using a caliper to measure a distance of about 2 cm between the chopper wheel and the TA converter. A scissor level is used to fine-tune the inclination angle of the TA system.
- Press the "Run" button on the speed controller to rotate the chopper wheel.
- Allow about 3 minutes to cool down the converter before collecting a new set of data by covering the lens completely to cease the solar flux heating the inside of the TA converter.
- Export the time domain data of the signal in the LabVIEW software and save it as an Excel file.
- All Excel files are examined using the MATLAB software.
- After collecting the data, reduce the speed of the chopper wheel slowly, then turn the generator off (cold chock) and disconnect all devices from the multi-

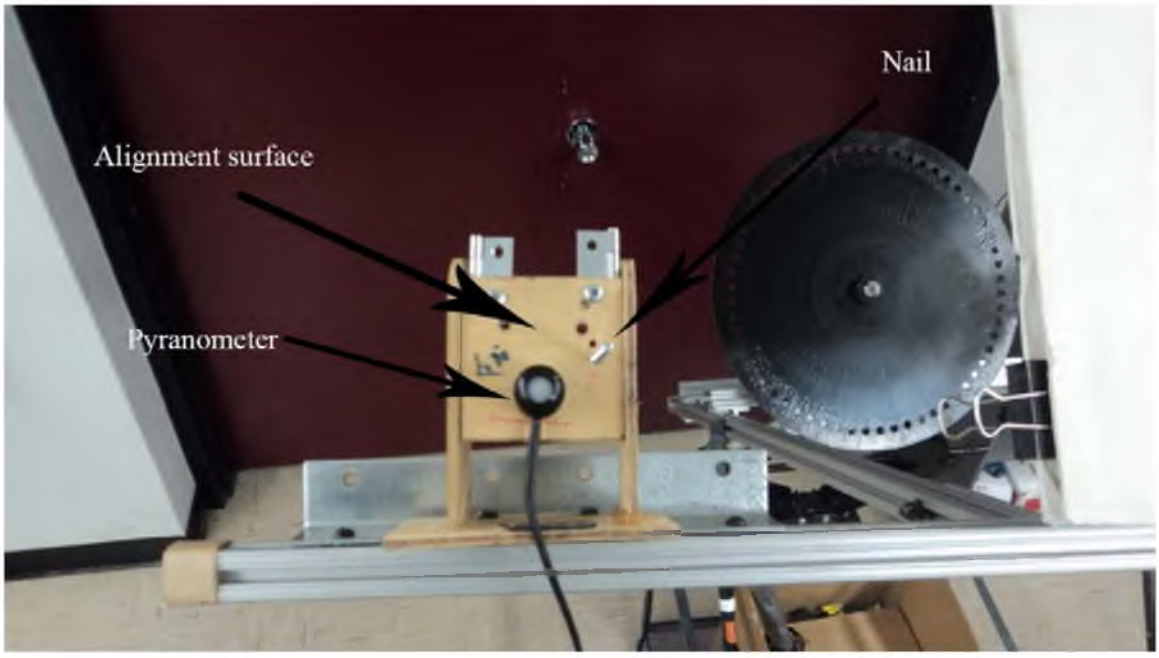

Figure 4.2 The pyranometer and alignment surface
used in this experiment.

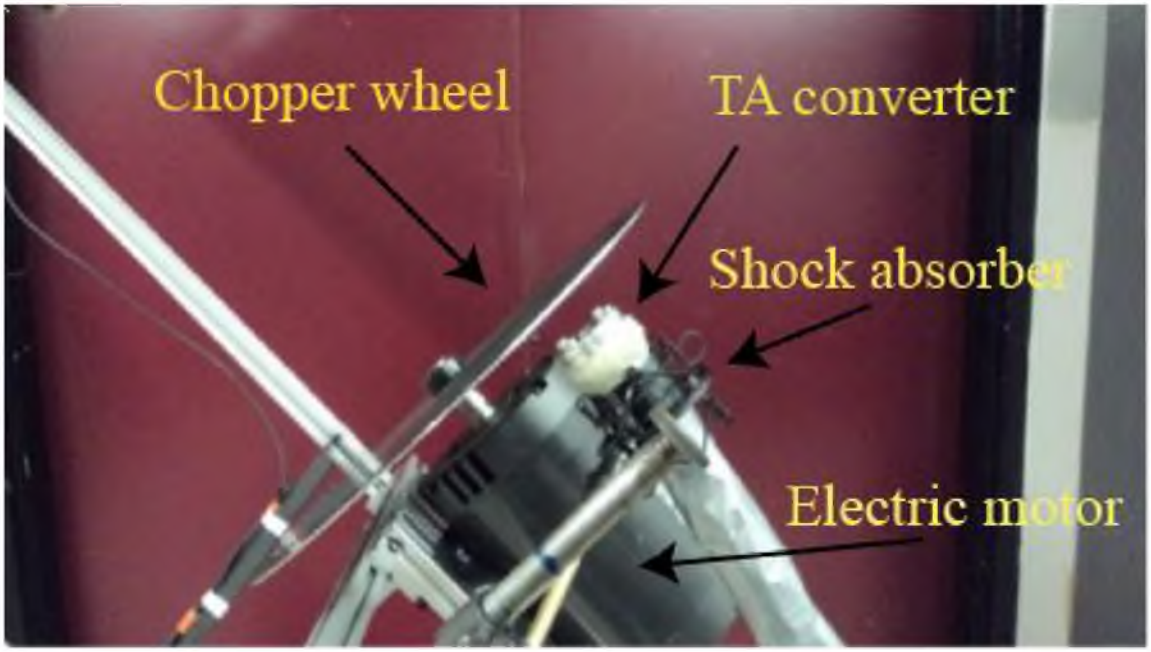

Figure 4.3 The alignment of the converter.

plug and turn the fuel flow off.

- Set the main switch of the generator off.

Figure 4.4 displays a diagram of the setup of the experiment.

4.3 Solar Radiation Reduction to Facilitate Sine Wave Production

In the first experiment, the amplitude of the TA signal was very high at low frequencies. This resulted in a truncated sine wave with a maximum microphone voltage around 4 V for frequencies less than 1 kHz. The author conducted an experiment to see if reducing the intensity of the solar radiation would result in an approximate sine wave. Two types of auto glass window tint films were used to shield the lens. The first film had a 30% heat reduction and 70% VLT (visible light transmission) [45]. This alone did not reduce the solar radiation enough, so a second type of window film was applied. The second window film had a 59% heat reduction and 40% VLT [38].

The combination of the first and second window films was successful in reducing the amplitude of the TA signal to approximately 3 V, resulting in the microphone signals closely resembling a sine wave for the frequency range of 200 to 860 Hz.

4.4 Signal Analysis

In this experiment, a closely sinusoidal wave should appear on the time domain data if the microphone has not reached its saturation level [6]. For this reason, the data revealed a truncated sine wave; the data was discarded.

The LabVIEW software is widely used in signal analysis. It was used to collect and visualize the data in this study. In addition to LabVIEW, MATLAB software was

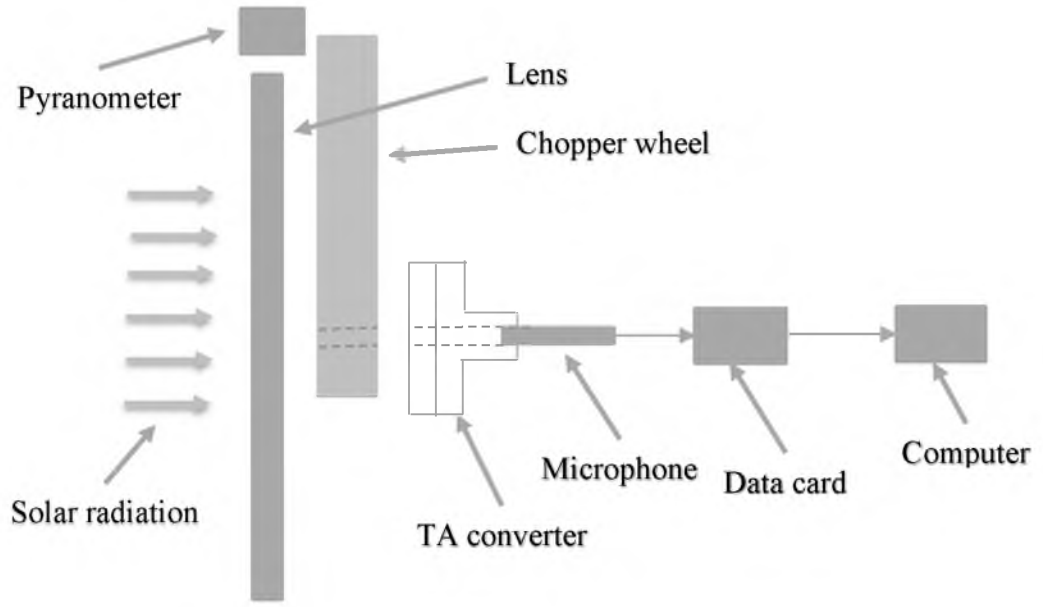

Figure 4.4 Diagram of the overall outdoor experiment

used to visualize and filter out noises and also used to convert time domain signals to frequency domain signals by using Fast Fourier Transform (FFT) analysis. More details the LabVIEW and MATLAB software appear in Appendix C.

4.5 Calibration Process

A calibration process was carried out in this study to convert the microphone signals from voltage to decibel, to elaborate and measure the loudness of the signal at specific frequencies, and to check the sensitivity of the microphone. Many tests were conducted to ensure the repeatability of these calibrations. The calibration process was comprised of two speakers, a microphone, and a data acquisition card that connected to the laptop. Following is the calibration procedure:

- Connect two speakers (Logitech speaker system z313) to the laptop.

- Turn the knob of the speakers to maximum.
- Set the computer speaker volume at 20%.
- Run a tone generator software. This software produces an acoustic signal with a sinusoidal wave at a specific frequency [46].
- Select desired frequency in the tone generator software.
- Increase the output level of the amplitude by using tone generator software tools (amplitude level option). The increment of an amplitude level should be consistent through the calibration process.
- Place the microphone (without insulation on it or inside the converter) in front of the speakers with 8.77 cm vertical distance and 30 degree angle toward the speakers as shown in Figure 4.5.
- Connect the microphone to the data acquisition card and then to the laptop.
- Put a sound pressure level (SPL) device (Tenma Company model #72-942) slightly above the microphone to measure the pressure variation in dBA unit. This device is used to measure the sound pressure with accuracy equal to $+/-$ 1.4–1.5 dB [47].
- The SPL device should be set on "hi-level, fast response, A-weighting" for general sound level (dBA) [47].
- Turn on the LabVIEW software and check the microphone amplitude RMS values (in Vs) simultaneously with SPL readings (in dBs) throughout the entire calibration process.
- Make a table of dBA values versus voltages values.

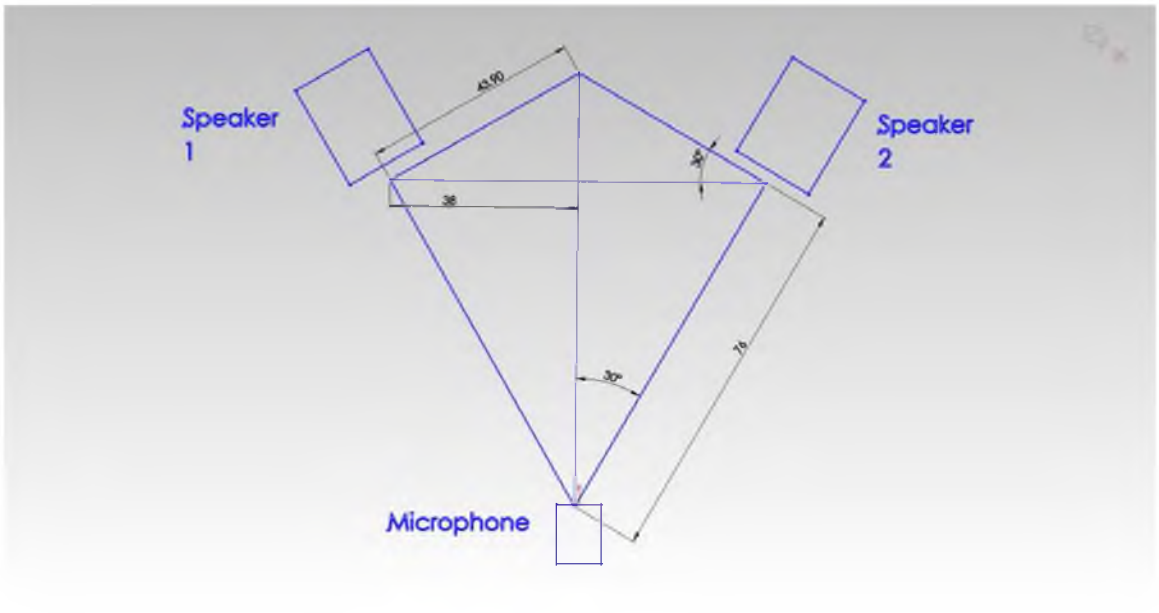

Figure 4.5 the overall calibration process schematic and illustrates the position of the two speakers and the microphone.

- Use the MATLAB software to plot the data. The filtration step is not necessary in the calibration process.

To convert the dBA units to dB, use an A-weight curve to obtain the dB unit by subtracting the dBA value at a specific frequency from the correction factor.

The Department of Clinical Science at Umeå University in Sweden used a microphone calibration system and procedure very similar to ours. Their system was comprised of a speaker, a sound pressure level meter, tone generator software, and a microphone in order to convert the volt unit to the dB unit. The distance between a microphone and the speaker is 15 cm and the sound pressure meter was positioned slightly above the mouth of the microphone (see Figure 4.6) [48]. Audioxpress also conducted calibration procedures by using a speaker and microphone. Audioxpress Company conducted a microphone calibration with a 16-inch distance between the

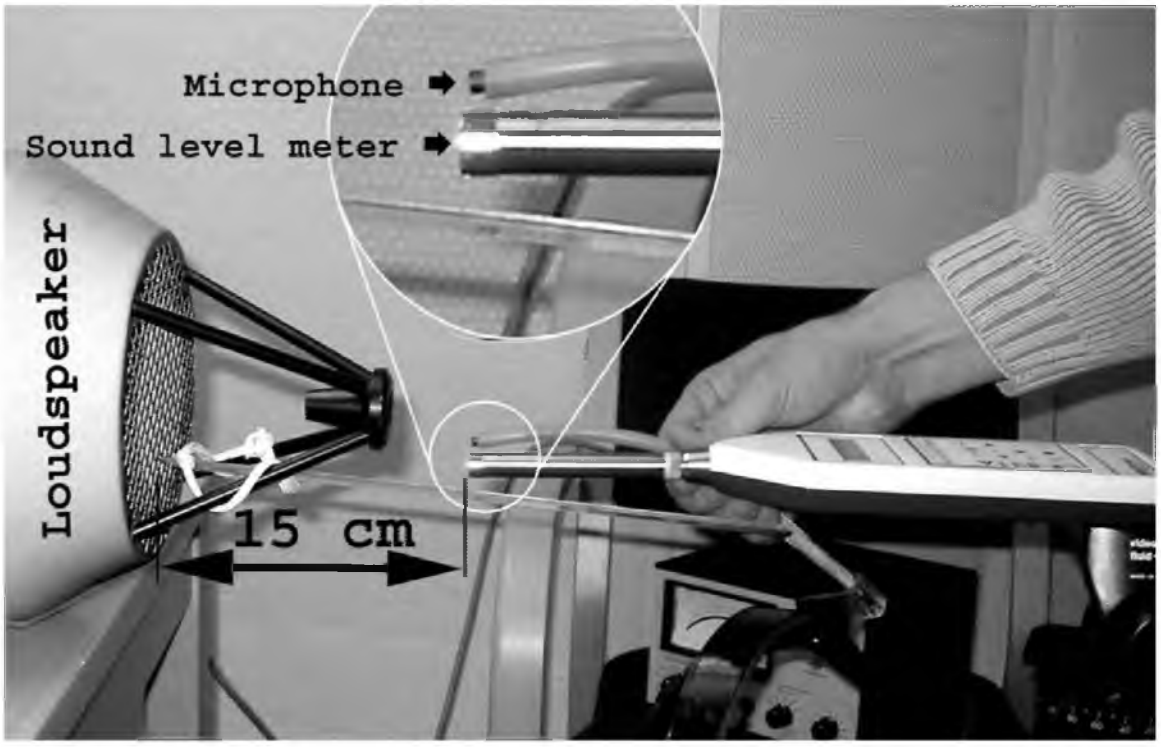

Figure 4.6 The calibration system and procedure and shows the position of a speaker, sound pressure level, and a microphone [48].

microphone and the speaker and showed the critical role on the microphone placement in their experiment [49].

The Department of Psychology and Language Science at University College London also used a microphone, speakers, and sound pressure level to calibrate their microphone [50].

In addition, Piezotronics Company used a microphone array technique to improve the quality of sound for their equipment by calibrating their equipment in front a numbers of microphones to extract background noise [51].

The calibration process at four specific frequencies (100, 400, 1000, and 3000 Hz) was conducted in order to compare it with the calibration plots of Rahman's thesis study.

The universal calibration plot from Rahman's study was used in this study because it included data for more frequencies. None of the calibration plots of this study exceed 3.5 V because the signal recorded by the microphone started to truncate above this level. This study confirmed Rahman's calibration plots and measured an average 3 dB difference between the calibration plots for this study and his plots. Appendix D shows Rahman's calibration data and curve fit formula for microphone voltage to dB converges. This calibration formula was based upon microphone data from 0.2 to 3.8 V. Extrapolation of this calibration curve was used for microphone voltage outside the range such as seen in Chapter 5 with dB units.

The time domain signal was expanded at these frequencies (100, 400, 1000, 3000 Hz) to show that the calibration plots in this study were conducted before the signal started to truncate. (See Appendices D and E for calibration plots and expanded signals.)

CHAPTER 5

RESULTS AND DISCUSSION

In this chapter, data collected in this thesis study are divided into two categories in order to separately examine the noise signals and the thermoacoustic signals that were generated due to radiation heating. First, background noise analysis was undertaken in order to study the behavior of the noise signals created when the TA converter was not heated before and after noise reduction methods were implemented. The purpose of this analysis is to separate the noise from thermoacoustic signals when the converter was heated. Second, thermoacoustic analysis was carried out to examine the behavior of the TA signals created when the TA converter was heated by pulsed solar radiation before and after noise reduction implementation. The effectiveness of the shock mount device, insulation materials, and new electric connections cables on the TA was investigated.

5.1 Noise Analysis and Reduction Without Radiation Heating

In order to improve the acoustic signal in this study, indoor and outdoor noise tests were performed before the inclusion of thermoacoustic effects. The purpose of these tests was to determine the background noises for different acoustic insulation conditions.

An indoor noise analysis experiment was first conducted in order to determine the background noises of the different cases mentioned below:

1. First test: Microphone exposed in front of two speakers for a wide range of frequencies (241 Hz to 3000 Hz), which shows that the microphone picked up high-amplitude noise between 3 V (or 77.8 dB) and 3.25 V (or 93.6 dB) depending on the frequency set in the tone generator software.
2. Second test: Microphone inserted inside converter without insulation materials and new cables. The noise signal was reduced significantly.
3. Third test: Microphone inserted inside converter with insulation materials and new cables. Background noise was only reduced slightly compared to case 2 for the same frequency range.

Figure 5.1 shows the noise amplitudes at different frequencies during the three tests. The results of the second and third tests show that the background noise was reduced significantly when compared to the signal of the microphone that was exposed to the surroundings, and it showed a small difference between the noise signals of the microphone inserted inside the converter with and without insulation on it. Noise sources in the lab might be: air conditioner, machine shop, and reflected sounds from the walls. The first test in Figure 5.1 shows that the amplitude of the two speakers starts decreasing from 214 to 860 Hz and then demonstrates a drop around 1000 Hz. This drop might be due to the output level of amplitude of tone generator software, which may change with frequency even though the level of the amplitude was fixed in tone generator software, or be due to the change in microphone sensitivity and/or properties with frequency.

Figure 5.2 presents only the results of tests 2 and 3 in order to show the relationship between frequency and amplitude more clearly for these two tests. The percentage difference of noise amplitude between these two tests is 18% for frequency

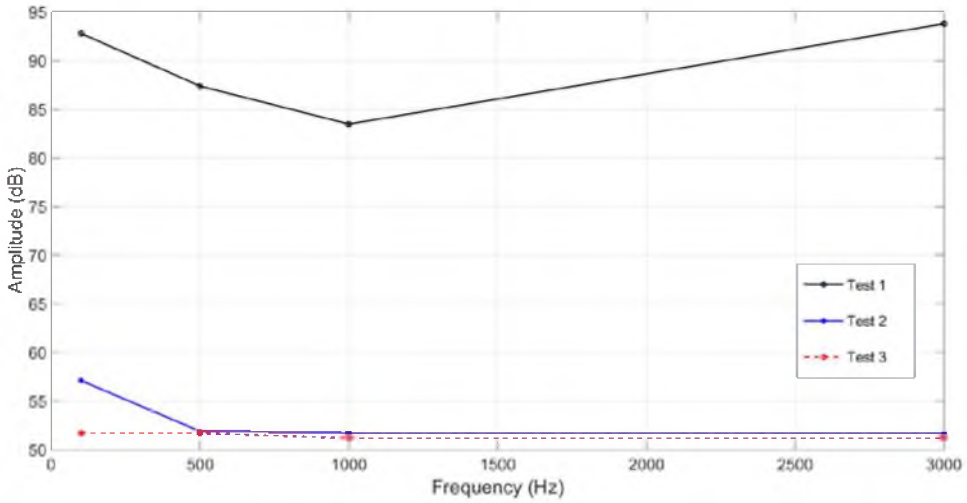

Figure 5.1 Indoor noise analysis (indoor tests) for three acoustic insulation conditions.

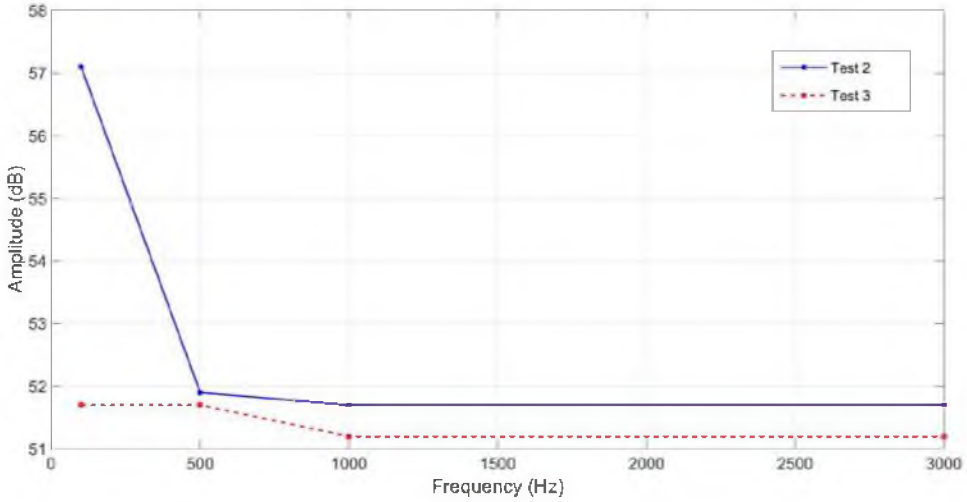

Figure 5.2 Results of tests 2 and 3 of the indoor experiment.

range 100–3000 Hz, but for frequency range 1000–3000 Hz the difference is only 8%. Figures 5.3, 5.4, and 5.5 show the amplitude of the noise signals for three different versions of the outdoor experiment that was conducted at the north-west corner of the MEB building, ground level, with no chopper wheel rotation. See Table 5.1 for more details about each case. The Figures from 5.3 to 5.5 show that the amplitude of the noise signal (RMS) for the outdoor experiment (mainly the noise generated by the electric generator) was measured to be 0.606 V (or 81.5 dB), as shown in Figure 5.3.

The noise amplitude was reduced to 0.466 V (or 80.4 dB) when the microphone was placed in the TA converter before noise reduction techniques, as shown in Figure 5.4. The noise was reduced to 0.030 V (or 66.4 dB) with the combination of shock absorption, insulation materials, and new electric connections applied to a more airtight TA converter, as shown in Figure 5.5.

Figure 5.6 shows an FFT analysis of noise recorded when the generator was turned on but the chopper wheel was turned off. The dominant frequency shown in this figure is 64 Hz (highest peak) with short peaks at 32 Hz and other very short peaks. The 64 Hz noise was also observed in the FFT analysis of the indoor experiment which had much less background noise. This frequency is an electric frequency [52], proving that the source of this noise is the electric circuit. As a result, in every noise analysis where a peak appears at 64 Hz, it can be attributed to electric noise.

Noise analysis after applying the noise reduction techniques (data from the experiments in 2015) is presented in more detail in the next section. Noise analysis required completely covering the lens so that no thermoacoustic effects occurred during this analysis. Only one microphone (inserted inside TA converter with noise

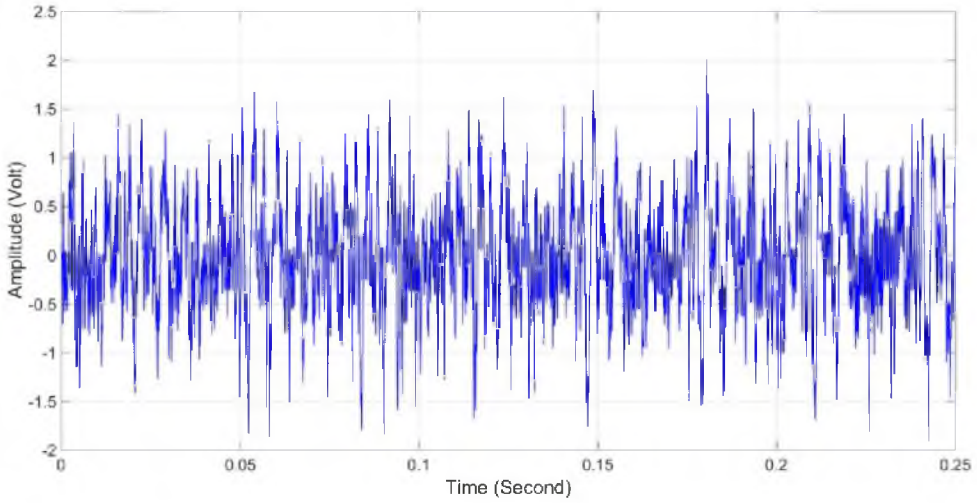

Figure 5.3 The noise signal generated when the microphone was exposed to surroundings.

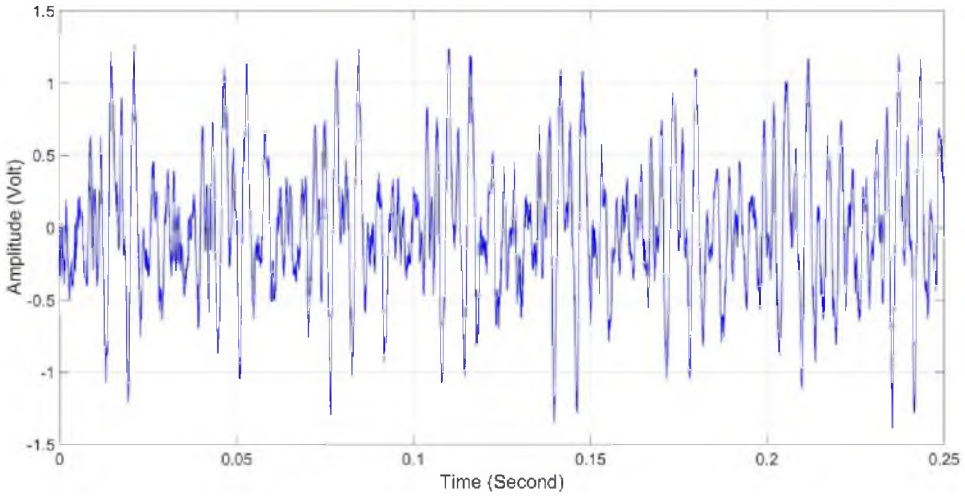

Figure 5.4 The noise signal of the microphone inserted inside the TA converter before implementation of noise reduction techniques.

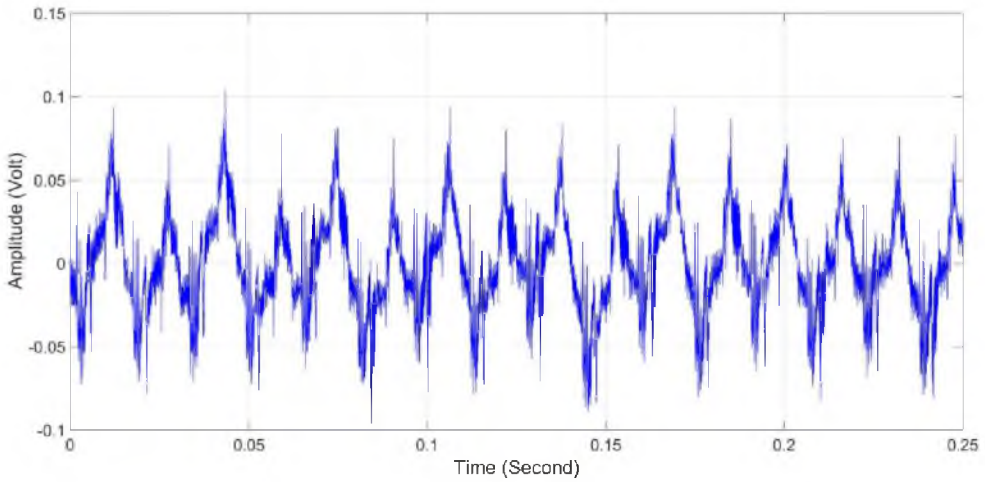

Figure 5.5 Generator noise signal when the microphone was inserted inside the TA converter after implementation of noise reduction techniques.

Table 5.1: Experimental conditions reflected in each of the outdoor noise signal analysis figures

	Elect. Generator	Microphone in the converter	Radiation heating	Insulation materials on converter
Fig 5.3	on	no	no	N/A
Fig 5.4	on	yes	no	no
Fig 5.5	on	yes	no	yes

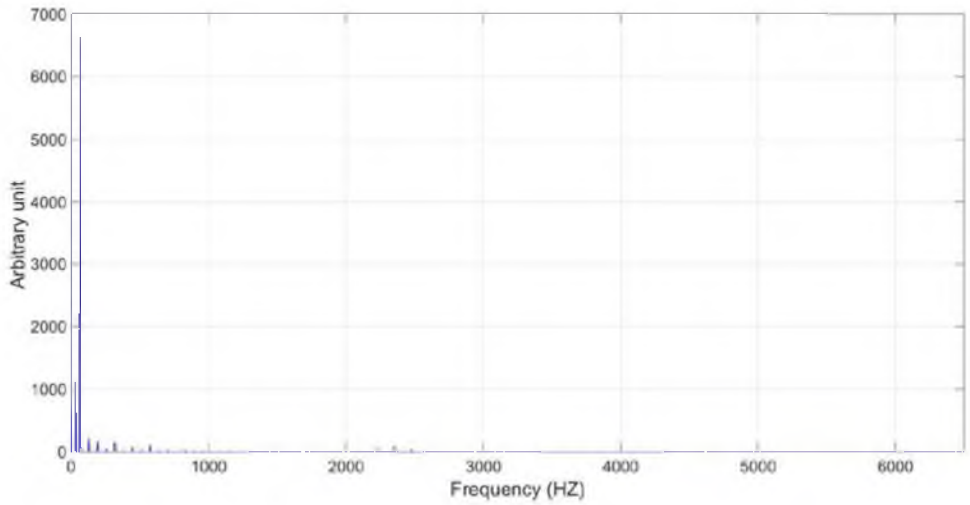

Figure 5.6 FFT analysis for noise signal when the generator was on.

reduction technique applied on it) was used to collect the data in 2015 to ensure consistency.

Figures 5.7 to 5.18 show time domain signal and FFT plots of the outdoor noise analysis with the chopper wheel turned on. In these cases, additional noises were generated due to the rotation of the chopper wheel and air flow over the holes in the chopper wheel. Figure 5.7 shows the amplitude of the signal (RMS value) at 241 Hz frequency (motor controller set on 4.01 RPS (revolutions per second) which indicates that the corresponding radiation beam frequency is RPS $\times$ 60 (number of holes in the chopper disk) = 241 Hz, if a radiation beam is interrupted by the chopper wheel) was 0.034 V (or 66.5 dB). The FFT plot in Figure 5.8 shows that the dominant peak was at 64 Hz with short peaks at 2001 Hz and 6002 Hz and several other very small peaks.

As can be seen in Figures 5.7 to 5.18, the RMS amplitude of the noise remained nearly constant at low chopper wheel speeds, and the dominant noise was electric noise at 64 Hz (see Figures 5.7 to 5.14). For chopper wheel speeds higher than 17 RPS (Figures

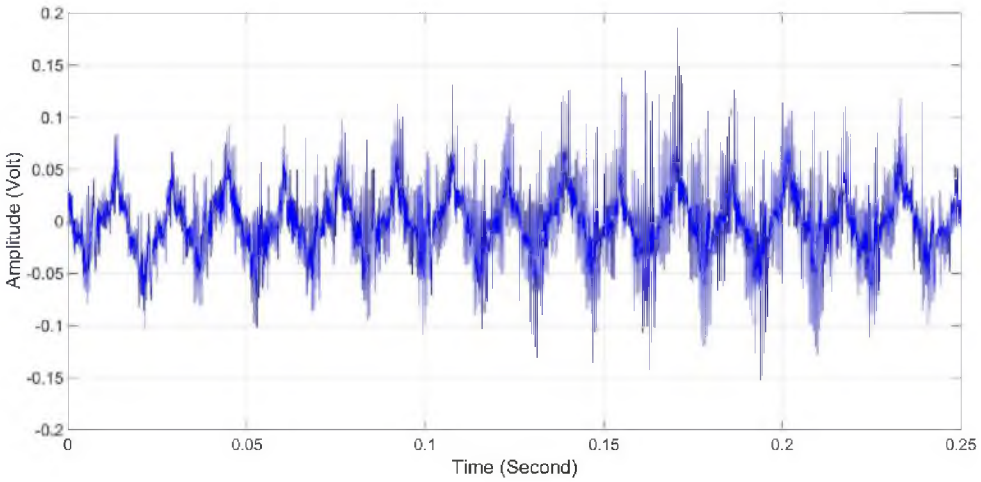

Figure 5.7 Noise signal of the generator, chopper wheel at 4.01 RPS. RMS amplitude was 0.034 V (or 66.5 dB)

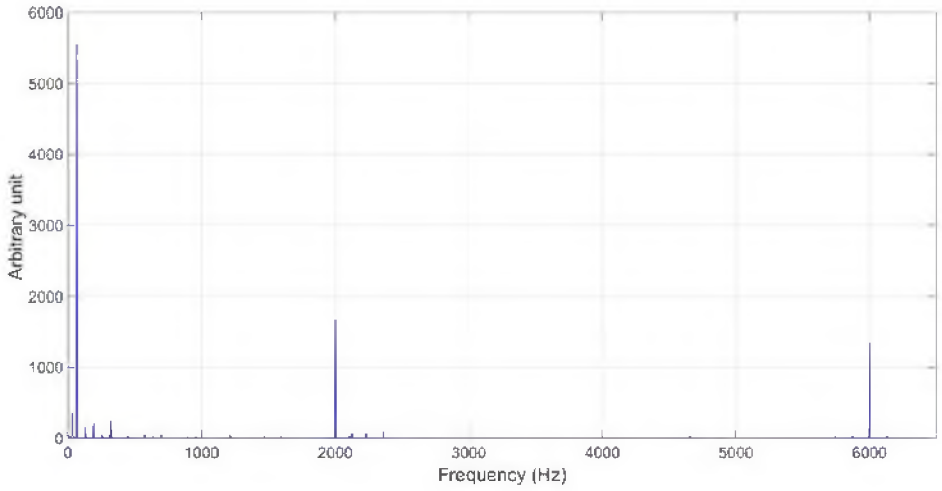

Figure 5.8 FFT analysis for noise signal at 4.01 RPS.

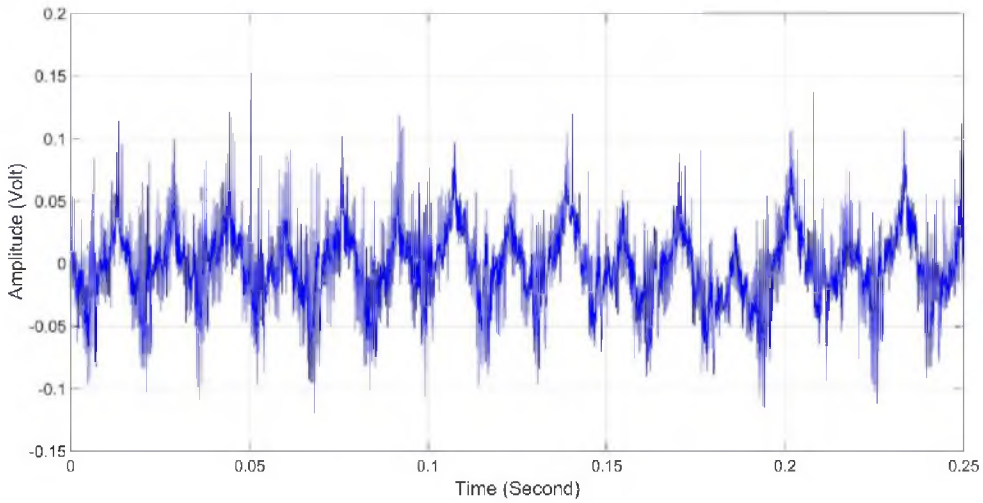

Figure 5.9 Noise signal with generator, chopper wheel at 7.51 RPS. RMS amplitude was 0.032 V (or 66.45 dB)

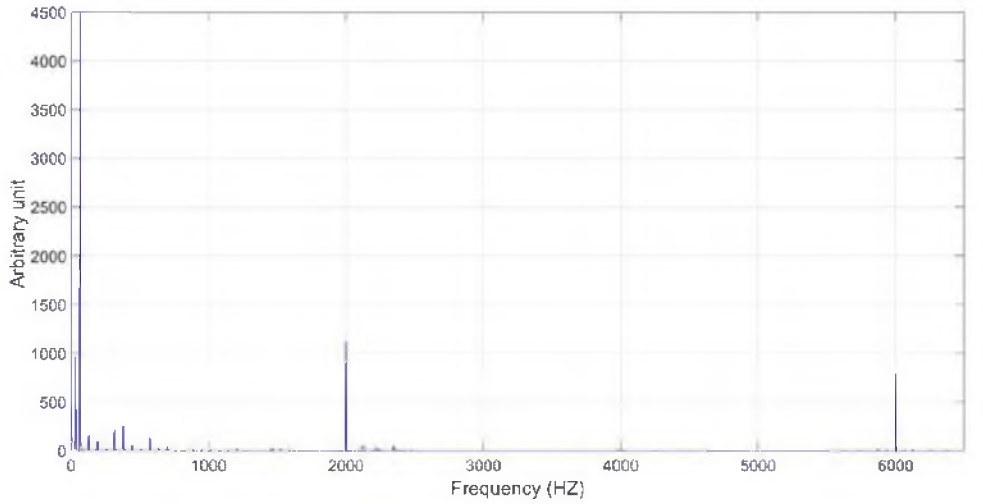

Figure 5.10 FFT analysis for noise signal at 7.51 RPS.

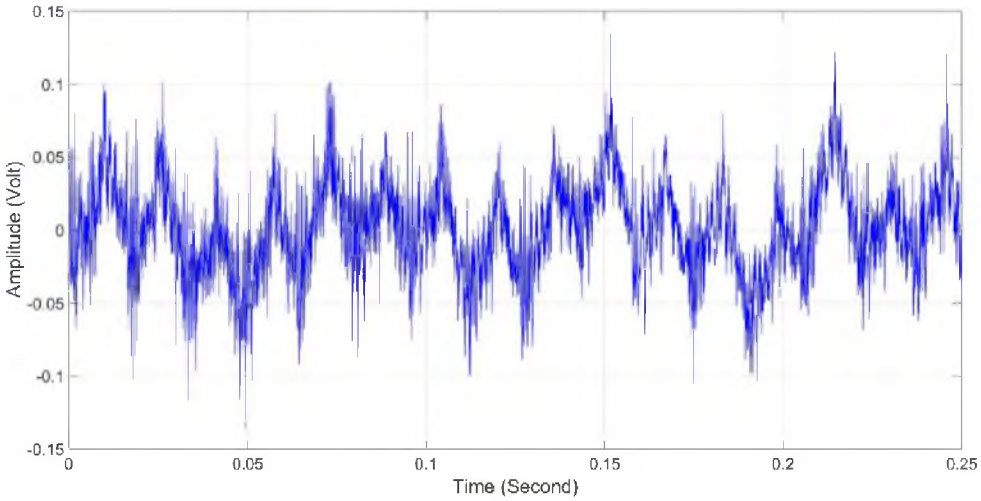

Figure 5.11 Noise signal with generator, chopper wheel at 14.33 RPS. RMS amplitude was 0.032 V (or 66.45 dB)

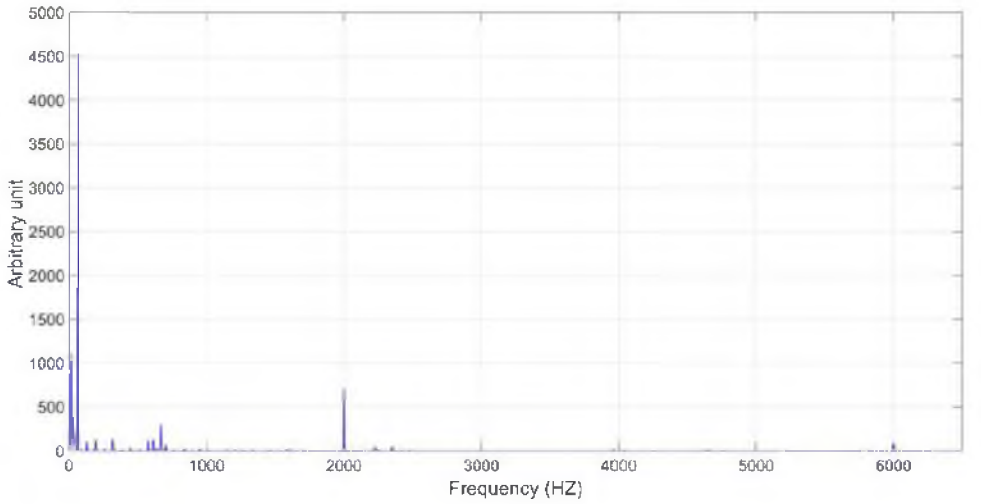

Figure 5.12 FFT analysis for noise signal at 14.33 RPS.

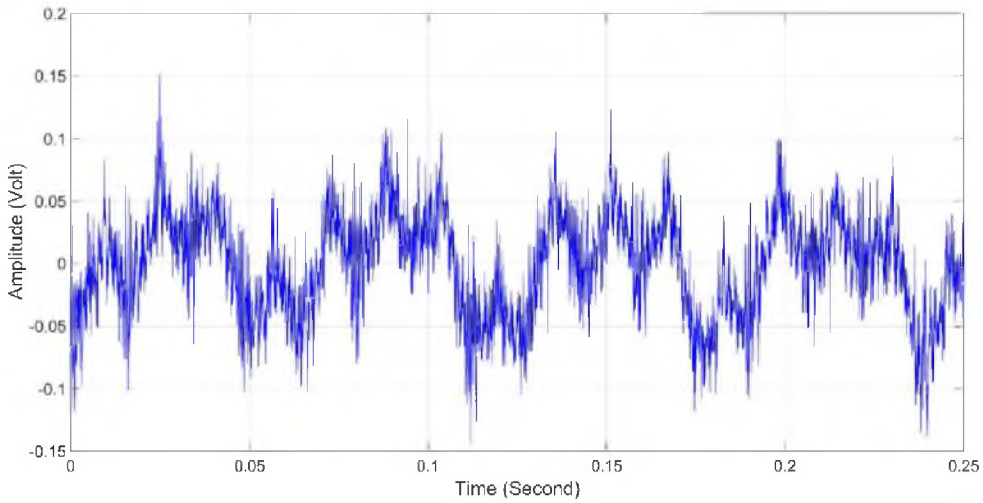

Figure 5.13 Noise signal with generator, chopper wheel at 16.66 RPS. RMS amplitude was 0.040 V (or 66.55 dB)

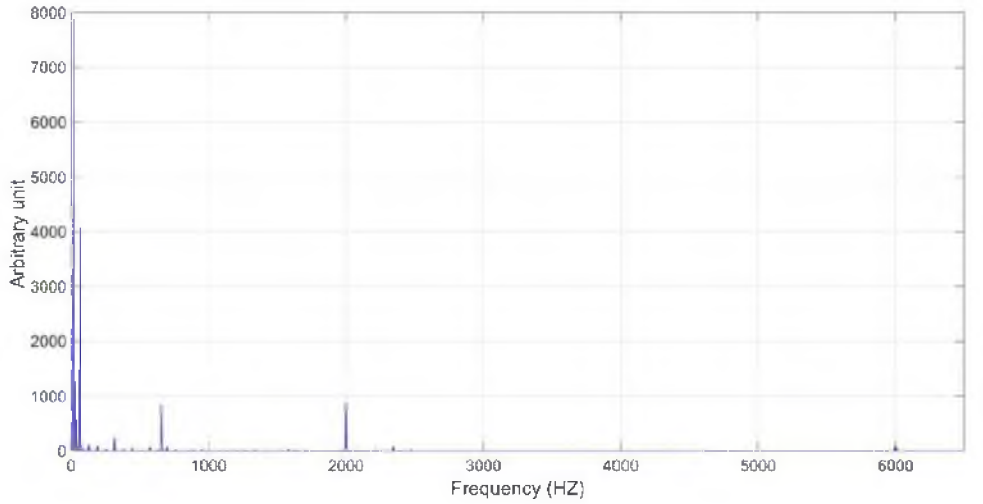

Figure 5.14 FFT analysis for noise signal at 16.66 RPS.

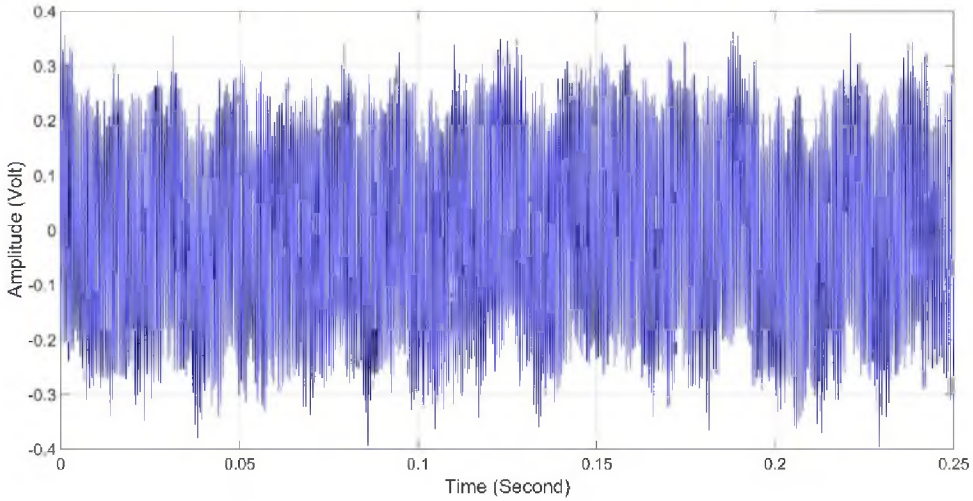

Figure 5.15 Noise signal with generator, chopper wheel at 41.88 RPS. RMS amplitude was 0.183 V (or 68.8 dB)

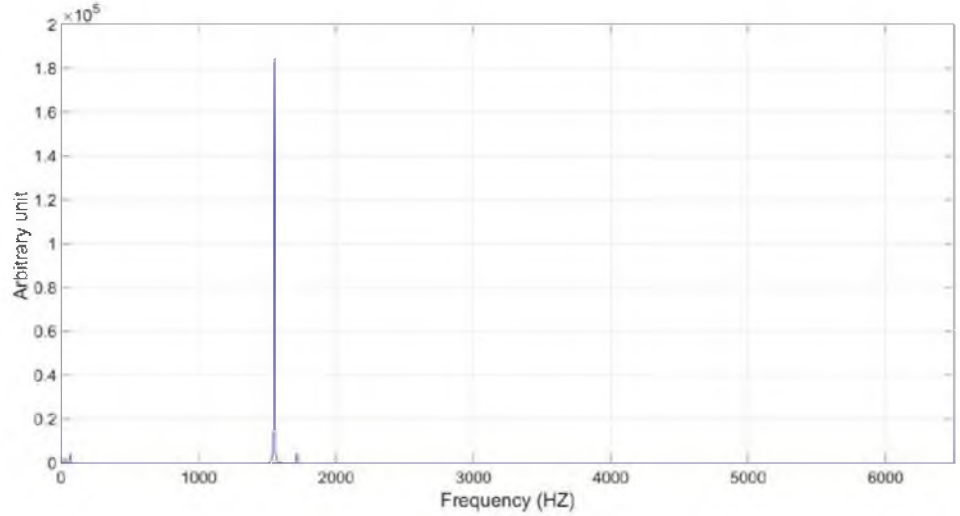

Figure 5.16 FFT analysis for noise signal at 41.88 RPS.

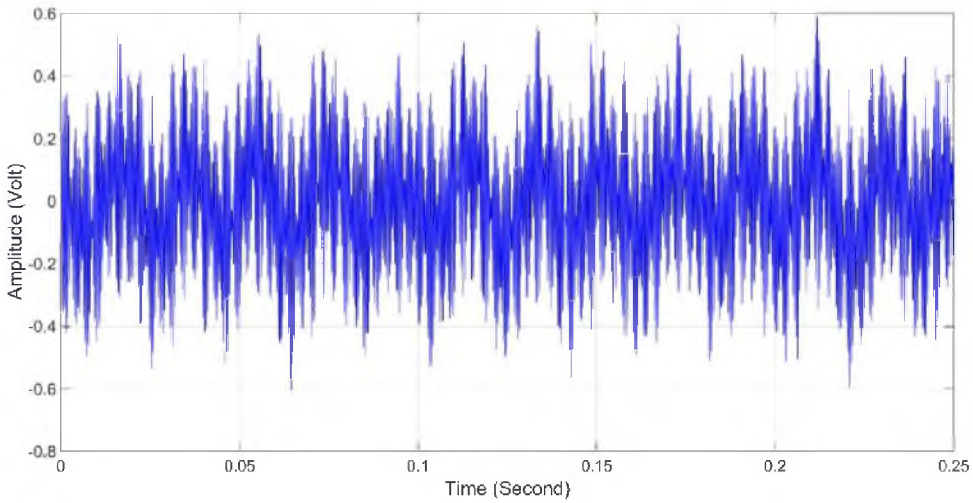

Figure 5.17 Noise signal with generator, chopper wheel at 50.33 RPS. RMS amplitude was 0.208 V (or 69 dB)

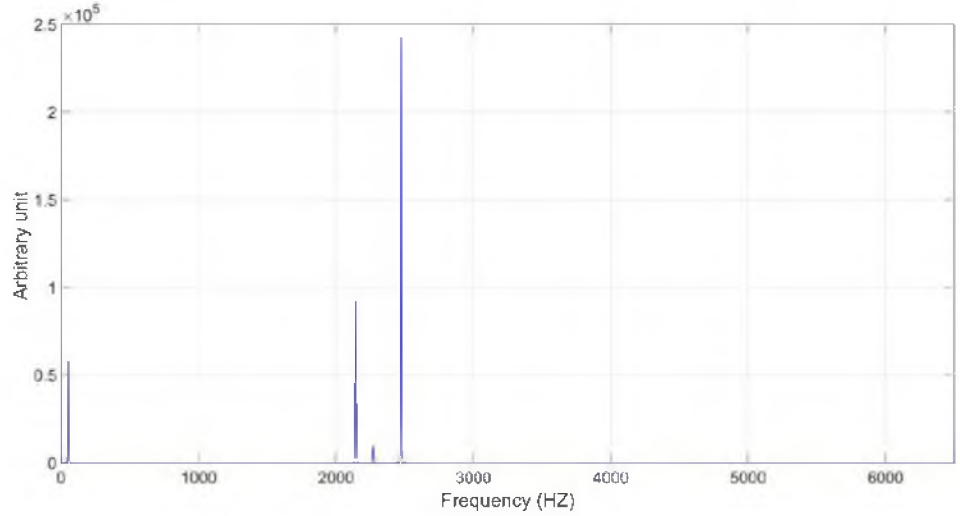

Figure 5.18 FFT analysis for noise signal at 50.33 RPS.

5.15–5.18), the noise amplitude increased rapidly with the chopper wheel speed, and noises in the kHz range become the dominant ones. These high-frequency noises were probably due to air flow over the holes in the chopper wheel.

It was observed that the noise waves consisted of both high- and low-frequency components. The low-frequency component can be seen clearly at low chopper wheel speeds (e.g., Figure 5.3 to 5.13) but is totally masked by the high-frequency component in Figure 5.15. There are two high-frequency components in Figure 5.17, as validated by the two tall peaks in Figure 5.18.

The FFT plots display electric noise at 64 Hz and a wide range of noises generated by the rotation of the chopper wheel. The results of the experiment verified the effectiveness of the shock mount device, insulation materials, and new electric connection cables in reducing the background noise to a minimum level.

Figure 5.19 shows the relationship between the noise amplitude and frequency after noise reduction techniques were applied to the converter system. The amplitude of the noise signal that was measured by the microphone placed inside the TA converter increased rapidly when the speed of the chopper wheel exceeded 16.66 RPS.

It is essential to determine the possible sources of outdoor noise. These might be the generator, wind, reflected signal from the wall, and rotation of the chopper wheel. The next section shows the noise analysis for three different outdoor tests:

1. First test: Microphone exposed to surroundings and placed behind the chopper wheel at a distance of about 2 cm. Results in Figure 5.20 indicate that the background noise during chopper wheel speeds of 4.01–50.33 RPS could be the noise from the generator and the rotation of the chopper wheel. The

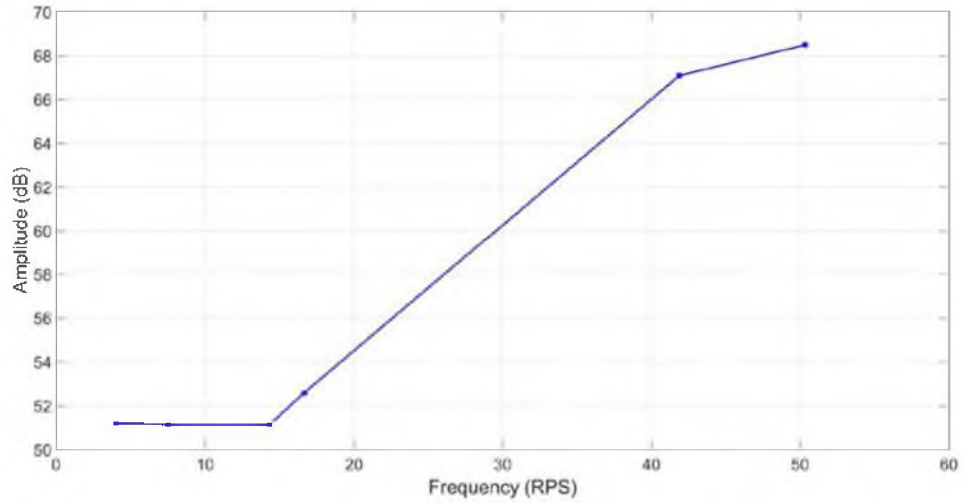

Figure 5.19 Relationship between frequency and the amplitude of the noise signal (outdoor experiment).

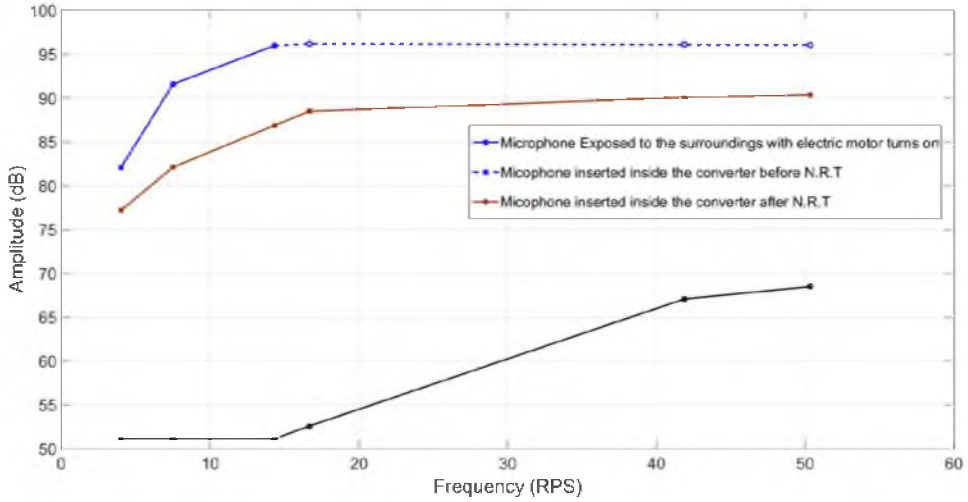

Figure 5.20 Noise signal analysis of the outdoor experiment for three different tests.

amplitude of the noise sources (mostly the generator, chopper wheel rotation, cart vibration, and wind) for the outdoor experiment first increased linearly and then began to approach a constant value. This indicates that the amplitude of the noise sources of the outdoor experiment increased when increasing the frequency of the chopper wheel before the microphone was saturated at about 4.5 V.

2. Second test: Microphone inserted into the converter, no other noise reduction techniques utilized. The background noise was reduced by 62% as compared to the first test. This test shows that the airtight design of the converter has a strong effect on noise reduction.
3. Third test: Microphone inserted into the converter after employment of noise reduction techniques. Compared to the second test, background noise was further reduced. The difference in clarity between the signals that were created in the converter in tests 2 and 3 was 93%. The curve of the third test in Figure 5.20 was based on the data in Figures 5.7–5.18.

5.2 Solar-to-Acoustic Energy Conversion

This section studies the thermoacoustic signals for a wide range of frequencies (241 to 3000 Hz) that were created by using pulsed solar radiation before implementation of noise reduction techniques.

Figure 5.21 shows that the amplitude of the TA signal decreased when increasing the frequency of the pulsed solar radiation within the range 241 Hz to 1000 Hz, but remained nearly unchanged for frequencies higher than 1000 Hz. These data were

collected from May to June, 2014 (12 noon to 2pm), and the solar intensity was around 1080 watt/m^2. The inverse relationship between frequency and amplitude in Figure 5.21 shows that the radiation absorption time is critical for generating acoustic waves. In other words, increasing the number of chopped cycles of the radiation beam caused the porous material in the converter per cycle to absorb less heat which reduced the air temperature variations inside the boundary layer (penetration depth of surface temperature fluctuation). As a result, when increasing the speed of the chopper wheel, the pressure variations inside the TA converter decreased and the sound had lower amplitude.

The data collected in June 2014 were not very consistent due to less experience in alignment. Variation in TA signal measurements varied from about 0.2 V at low frequencies, to about 0.5 V at frequencies above 1 kHz.

5.2.1 Time Domain Signals and FFT Analysis After Implementing Noise Reduction Techniques

This section presents thermoacoustic converter signals after applying a shock mount device, insulation materials, and replacing the electric connection cables. These data were collected from Feb–Apr, 2015 (12 noon to 2pm) and the solar intensity was between 1060 to 1080 watt/m^2.

Figure 5.22 shows that the amplitude of the thermoacoustic signal was about 5 V (or 95 dB) at 241 Hz (frequency of the chopped radiation beam). Figure 5.23 is the FFT of Figure 5.22. Figures 5.24 and 5.25 are the unfiltered TA signal and its FFT at 860 Hz. A close inspection of the wave forms reveals that the measured sound waves were truncated sine waves for frequencies less than 1000 Hz, indicating that the sound

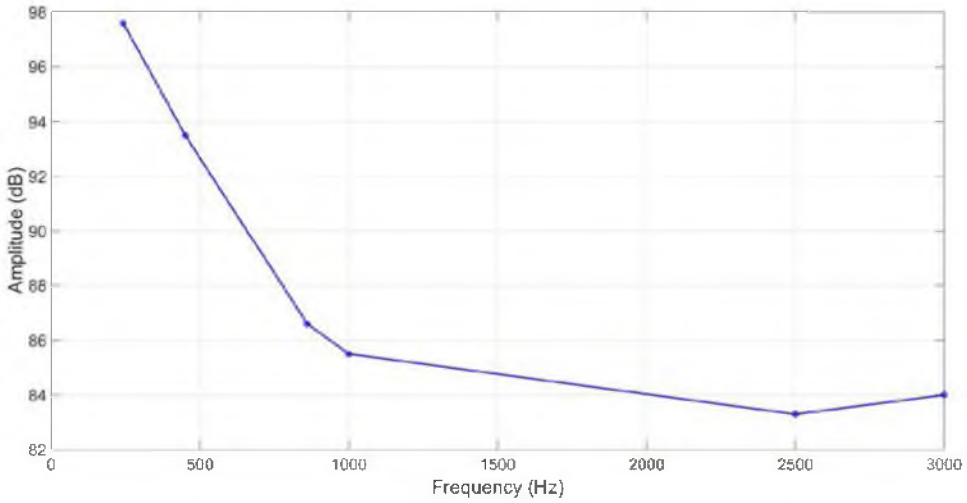

Figure 5.21 The thermoacoustic signal of the outdoor experiment within a wide range of frequencies before implementing noise reduction techniques.

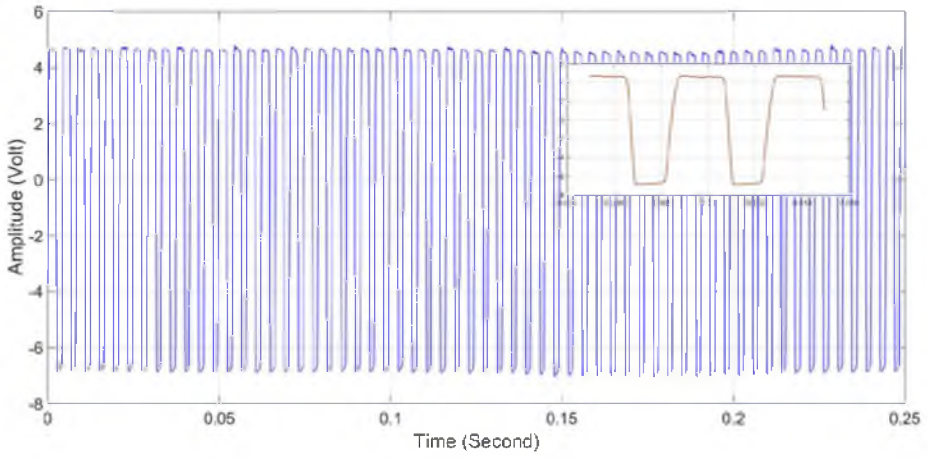

Figure 5.22 Unfiltered thermoacoustic signal at 241 Hz frequency.

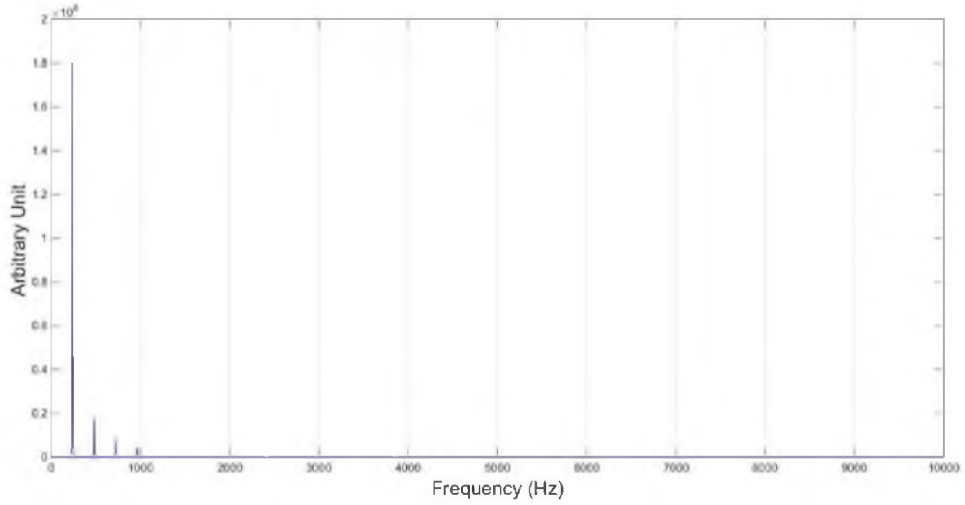

Figure 5.23 FFT analysis for unfiltered thermoacoustic signal at 241 Hz.

generated inside the converter was very loud at low frequencies. The microphone had reached its saturation level (threshold level) in these cases.

In the kHz frequency range (Figures 5.26–5.31 display the unfiltered thermoacoutic signals and the results of the filtered FFT analysis), the maximum amplitude dropped below 4 V and the wave form was no longer truncated. The wave forms which were not truncated closely resembled a sinusoidal wave. The amplitude of the signal continued to reduce as the frequency of the chopped radiation increased for frequencies greater than 1000 Hz. This is the major difference between TA signals before (Figure 5.21) and after noise reduction.

Since the truncated waves at 241 Hz resemble a square wave, the FFT plot of 241 Hz shows several peaks. In other words, the square wave is a superposition of sine waves of different wave lengths. On the other hand, FFT plots of 860 to 3000 Hz have only one dominant frequency, indicating the wave form closely resembled a sinusoidal wave.

Figure 5.32 shows the relationship between the sound amplitude and frequency of

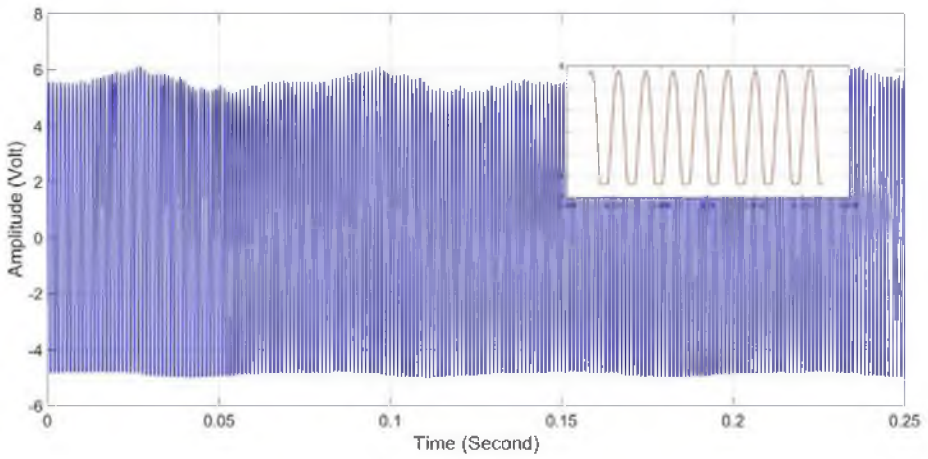

Figure 5.24 Unfiltered thermoacoustic signal at 860 Hz frequency.

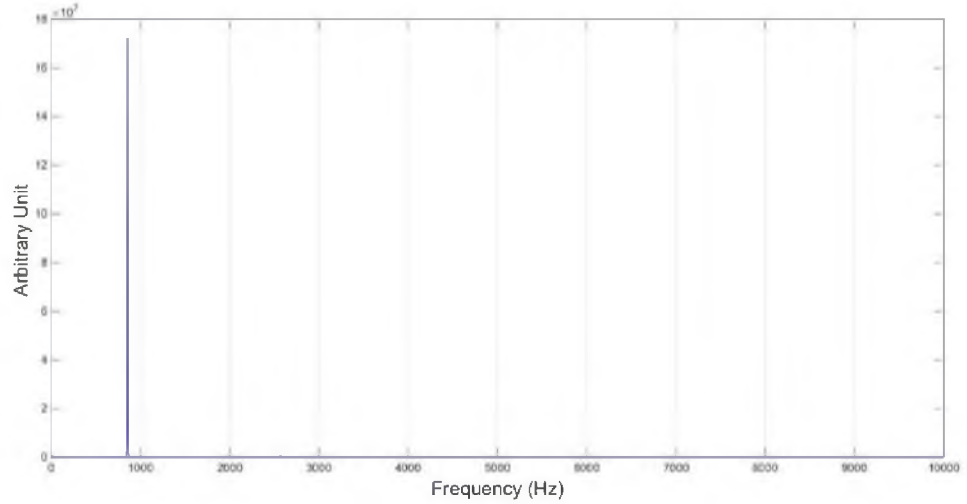

Figure 5.25 FFT analysis for the thermoacoustic signal at 860 Hz.

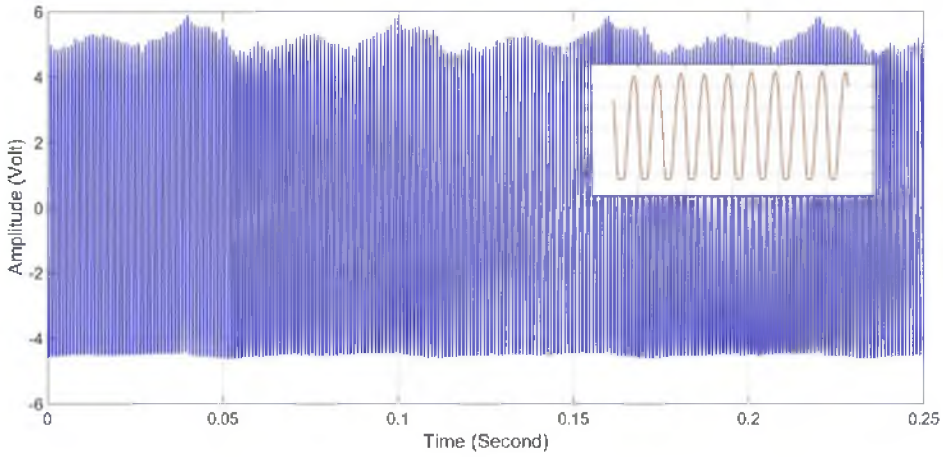

Figure 5.26 Unfiltered thermoacoustic signal at 1000 Hz frequency.

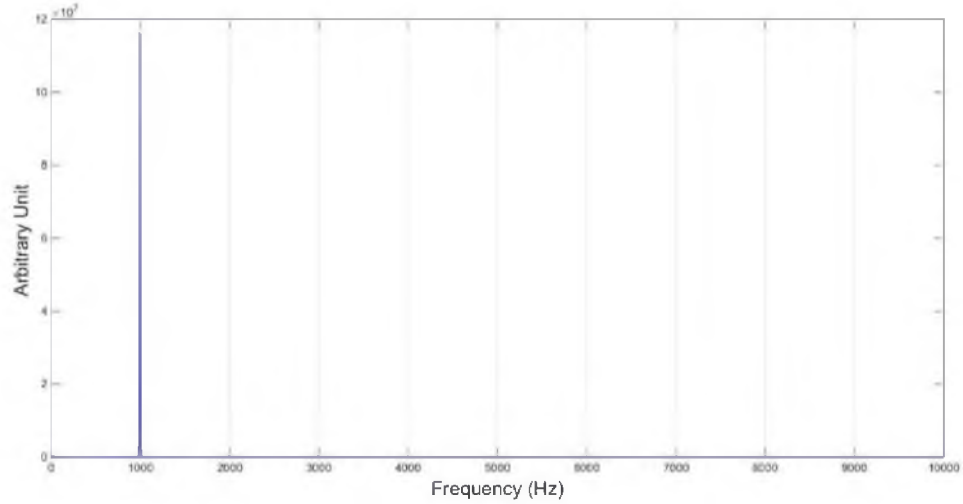

Figure 5.27 FFT analysis for thermoacoustic signal at 1000 Hz.

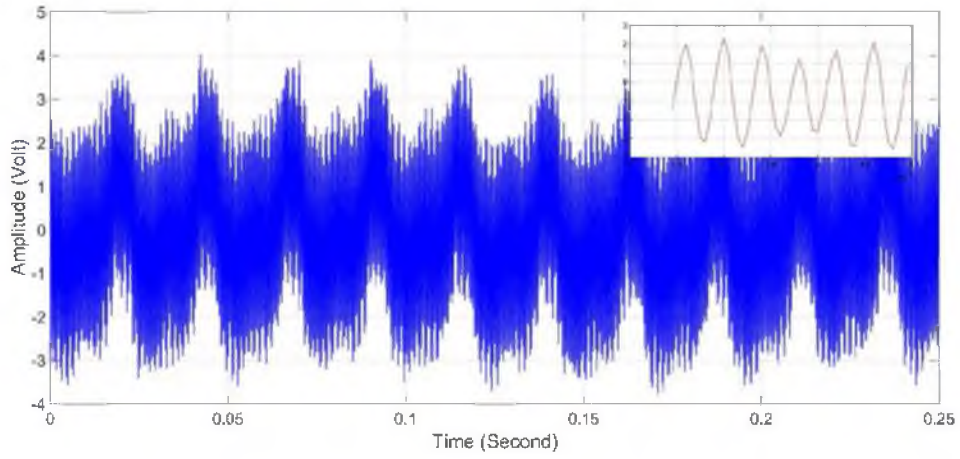

Figure 5.28 Unfiltered thermoacoustic signal at 2.5 kHz frequency.

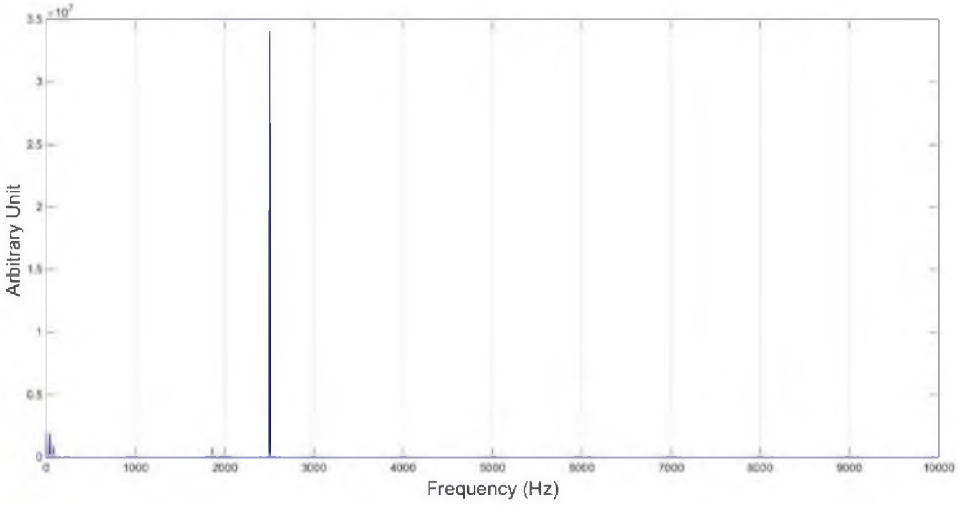

Figure 5.29 FFT analysis for the thermoacoustic signal at 2.5 kHz.

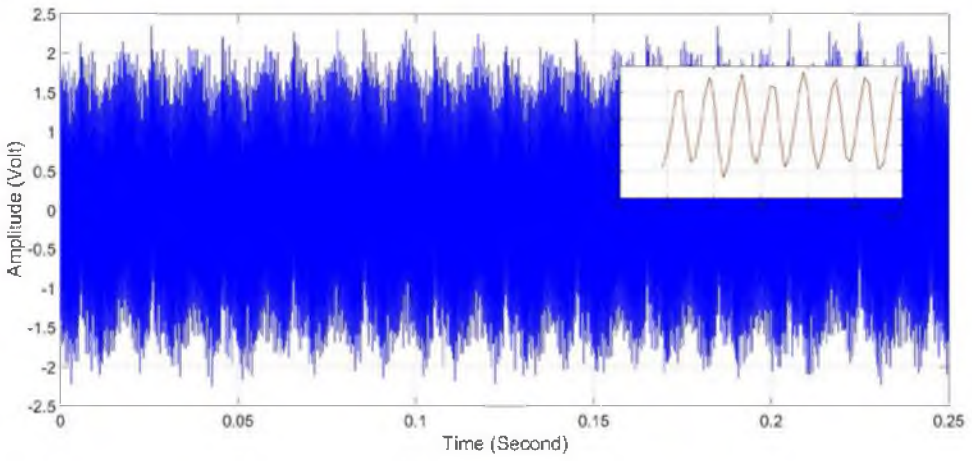

Figure 5.30 Unfiltered thermoacoustic signal at 3 kHz frequency.

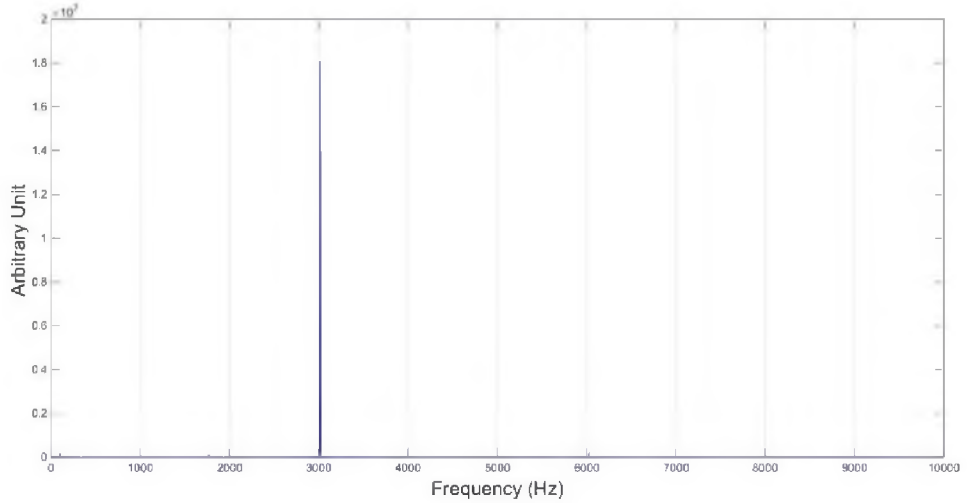

Figure 5.31 FFT analysis for the thermoacoustic signal at 3000 Hz.

the thermoacoustic signal after noise reduction. The sound amplitude decreases nearly linearly when increasing the speed of the chopper wheel which increases the pulsed radiation frequency. The absorption time of the solar radiation inside the TA converter reduces when increasing the speed of the chopper wheel. It should be kept in mind that amplitudes for frequencies less than 860 Hz in Figure 5.32 are lower than they should be since the sound waves were truncated.

Table 5.2 lists the measured microphone signals and the pure thermoacoustic signals after subtracting the noise for pulsed frequencies from 241 to 3000 Hz.

Because of the truncated waves for frequencies less than 860 Hz in the first experiment, a new experiment was designed to generate sound waves which were not truncated at low frequencies. In the new experiment, auto glass window tint films were used to reduce the solar intensity. Figure 5.33 shows the results of the tests with the auto glass films.

Case 1: No films were applied to the lens. Only the amplitudes of TA signals in kHz frequency range (1000 to 3000 Hz) were considered for Case 1 because only the signals in this range closely resembled a sinusoidal wave. Case 1 shows that the amplitude of the TA signal decreased linearly when increasing the frequency of the chopper wheel.

Case 2: One film was applied to the lens. The film achieved 30% heat reduction and reduced the amplitude of the TA signal by 8%. TA signal data below 1 kHz were disregarded for Case 2 since the wave forms were still found to be truncated at low frequencies. As in Case 1, the amplitude of the TA signal decreased linearly when increasing the frequency of the chopper wheel for the kHz range, but when the frequency

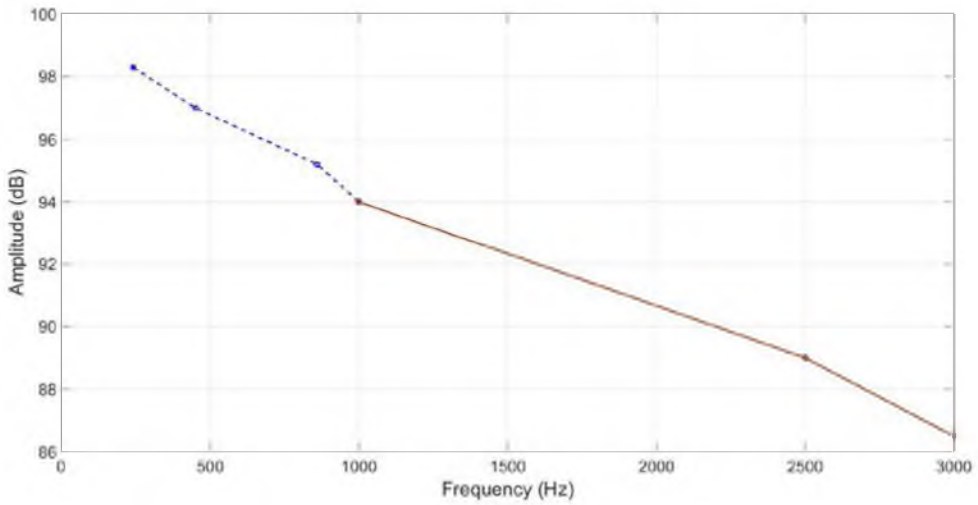

Figure 5.32 Thermoacoustic signal of the 2015 outdoor experiment

Table 5.2: The amplitude of the TA signal within frequency range 241–3kHz.

Frequency (Hz)	Measured signal (unfiltered TA) (V)	Noise signal (V)	Pure signal (V)
241	5.17	0.034	5.13
451	4.939	0.032	4.90
860	4.14	0.032	4.10
1000	3.72	0.040	3.68
2500	1.82	0.183	1.63
3000	1.23	0.208	1.02

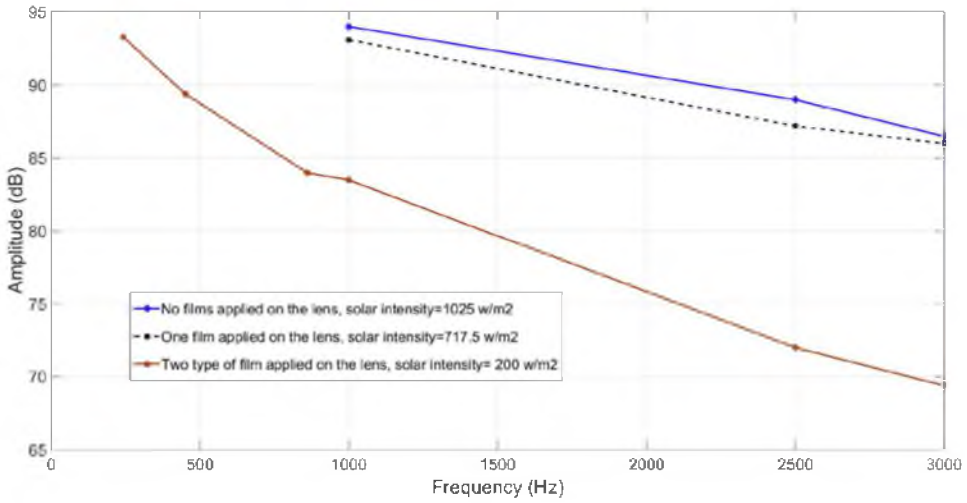

Figure 5.33 The relationship between sound amplitude of the TA signal and the frequency for three different cases

reached 2500 Hz, the rate of decrease slightly leveled off.

Case 3: A second film was added to the lens. This film added 60% heat reduction. With the combination of the two films, the relationship between the amplitude of the signal and the frequency of the chopper wheel in the low-frequency range decreased almost exponentially. Above 1000 Hz, the relationship became linear. At 3000 Hz, the amplitude of the TA signal was 0.239 V. Comparing the amplitudes in Figure 5.33, it is clear that reducing solar intensity has a significant impact on the amplitude of the sound generated by the converter.

5.2.2 Transient Behavior of the Thermoacoustic Signal

The next section presents the transient behavior of the thermoacoustic signal. An experiment was conducted to examine the change in the amplitude of the TA signal at a pulsed radiation frequency equal to 241 Hz with and without a film applied to the lens.

Figure 5.34 shows the amplitude change (in RMS) of the TA signal at 241Hz when the film that provided 30% radiation reduction was removed from the lens after approximately 6 seconds. At the moment of removing the film, the amplitude of the TA signal started to increase rapidly. This rapid increase of amplitude took about 1 second and then started to decrease slightly. After 1 more second, the amplitude started to approach an almost steady state. This observation of transient behavior in the TA signal is in agreement with Rahman's indoor experiment data and the reason for the behavior has been discussed in his thesis.

5.2.3 Digital Filter Analysis in MATLAB

A MATLAB code was developed to digitally filter out some noises for improved signal-to-noise ratio. Figures 5.35–5.47 display the results of this analysis. TA signals from the outdoor experiment were passed through a digital high pass filter in the MATLAB program with a cut off frequency of 70 Hz for pulsed frequencies 241–450 Hz, and 500 Hz for 860–3000 Hz. In addition to this high pass filter, a low pass filter with a cut off frequency of 300 Hz was also used for 241 Hz in Figure 5.42 to eliminate the peaks above 300 Hz for the truncated sine wave in Figure 5.41. Figures 5.41–5.47 display the results of the filtered FFT analysis.

In order to explain the curve trend in Figure 5.33, Fourier number was calculated in this study to assess the penetration of filament surface temperature fluctuation into the air in steel wool.

The Fourier number is the ratio of the heat conduction rate to the rate of thermal energy storage in a solid [53].

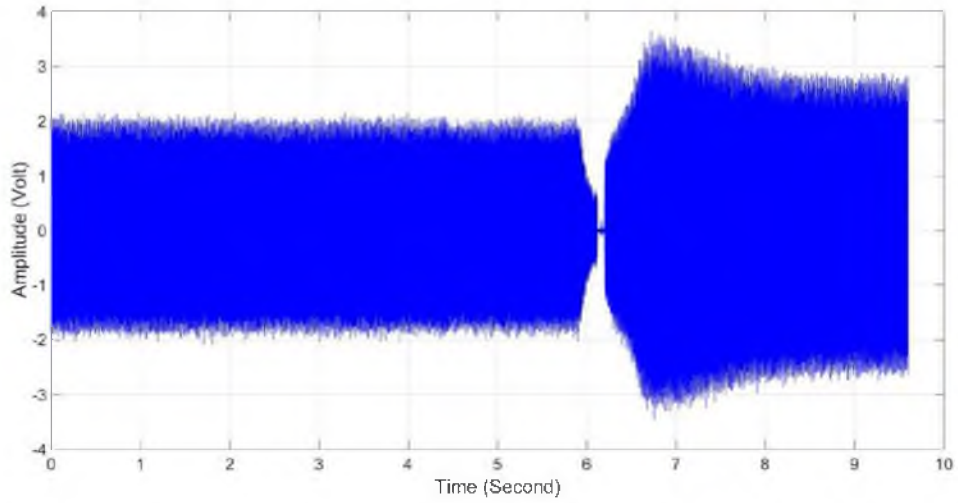

Figure 5.34 The time domain signal at 241 Hz before and after removing from the lens the film that provided 30% radiation reduction.

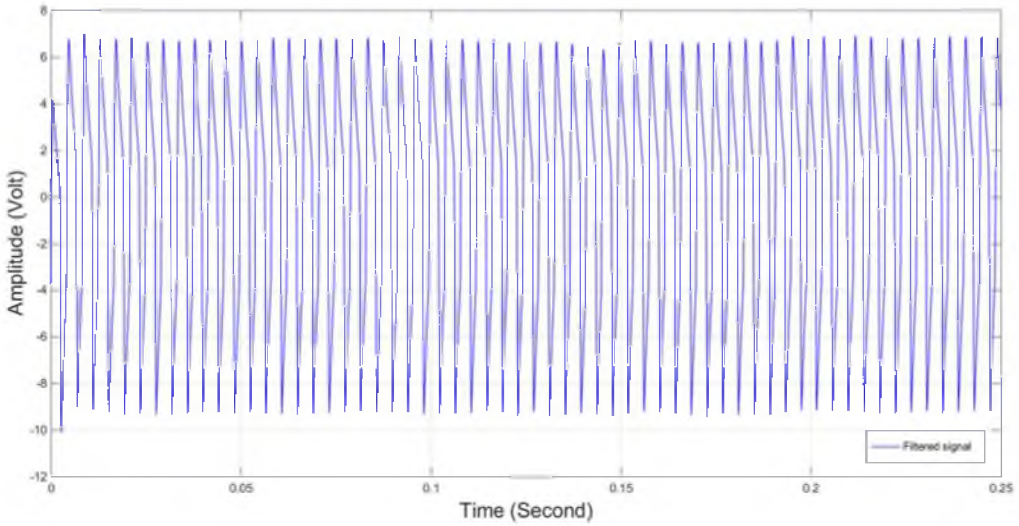

Figure 5.35 Filtered TA signal at 241 Hz.

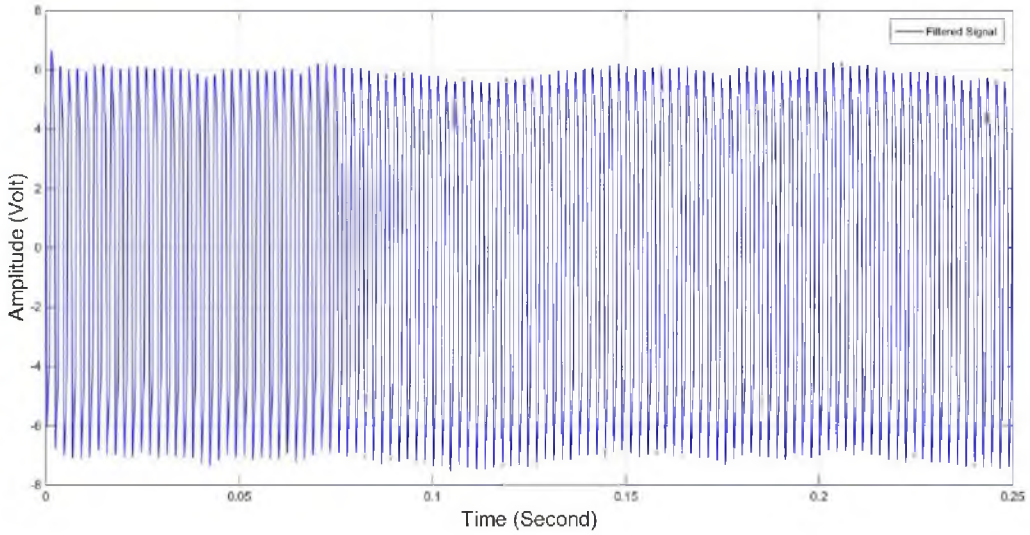

Figure 5.36 Filtered TA signal at 451 Hz.

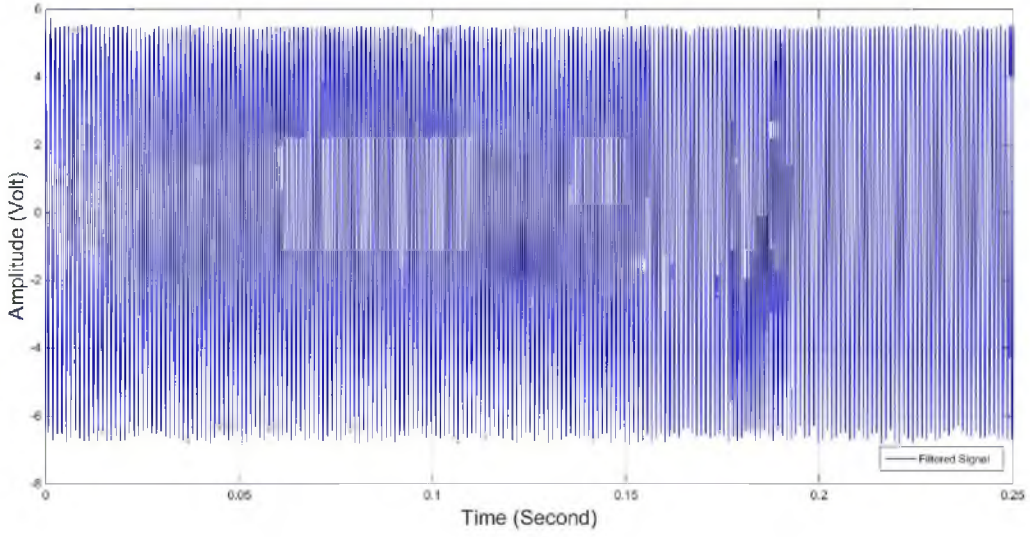

Figure 5.37 Filtered TA signal at 860 Hz.

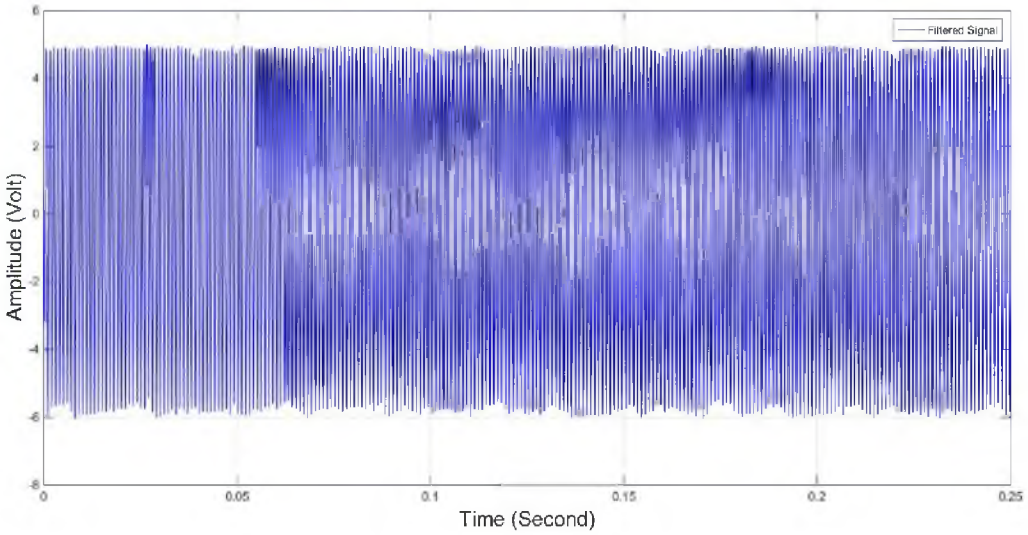

Figure 5.38 Filtered TA signal at 1000 Hz.

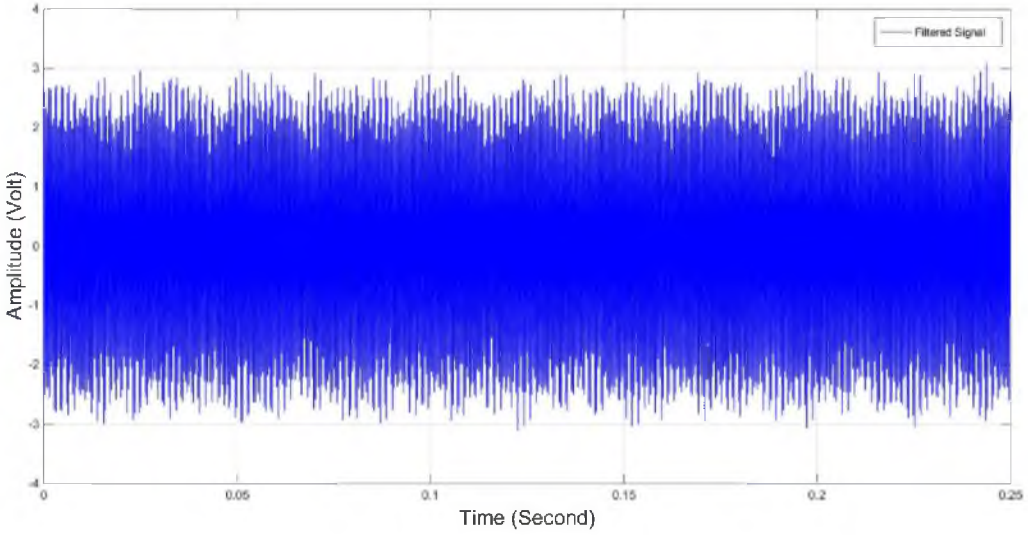

Figure 5.39 Filtered TA signal at 2500 Hz.

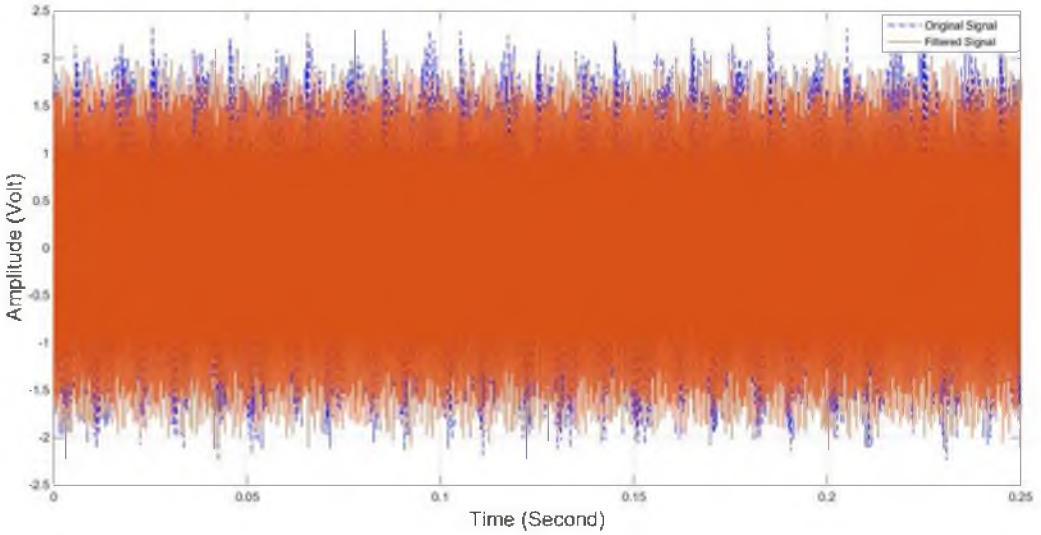

Figure 5.40 Filtered TA signal at 3000 Hz.

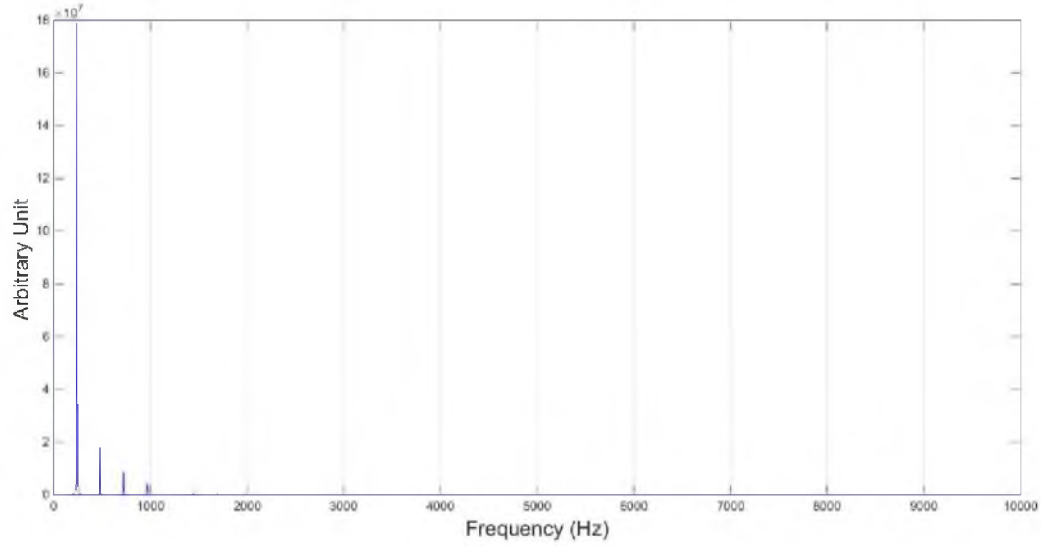

Figure 5.41 Filtered FFT analysis at 241 Hz.

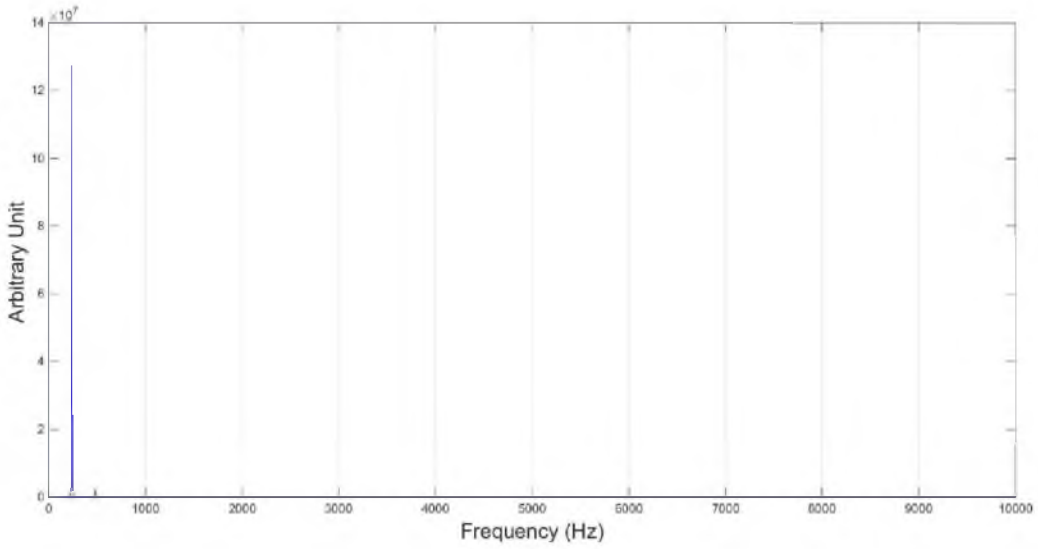

Figure 5.42 Filtered FFT analysis at 241 Hz with different types of filters.

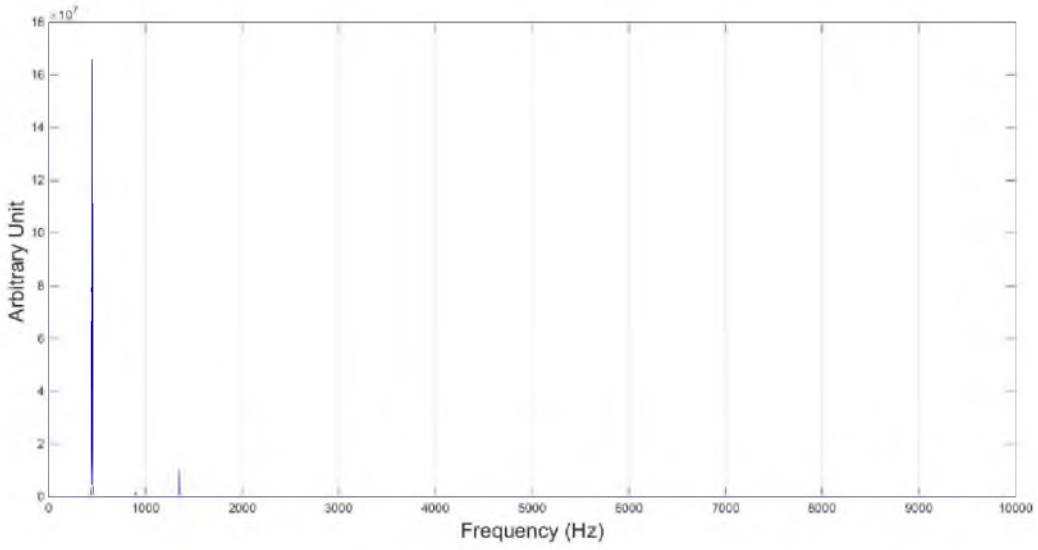

Figure 5.43 Filtered FFT analysis at 450 Hz.

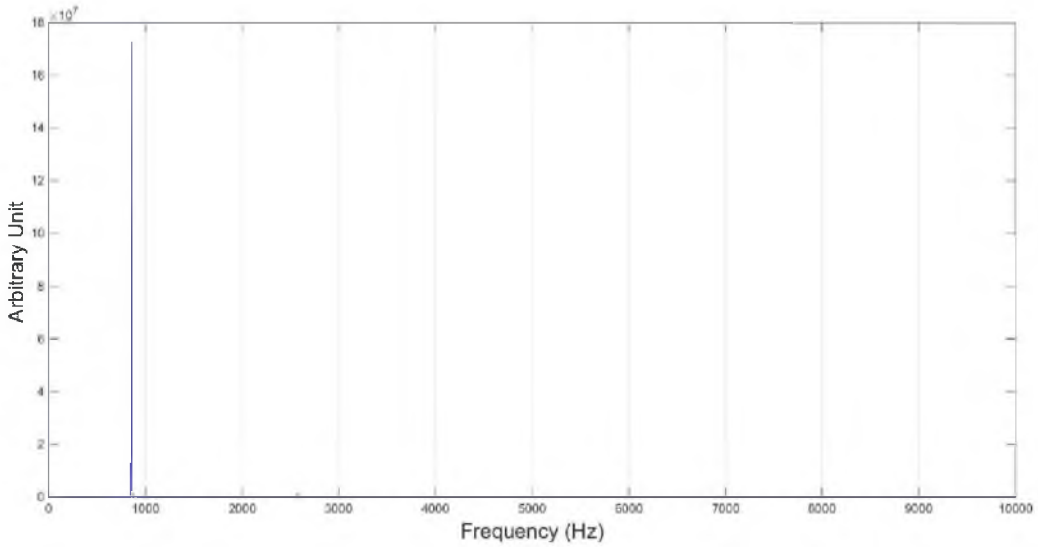

Figure 5.44 Filtered FFT analysis at 860 Hz.

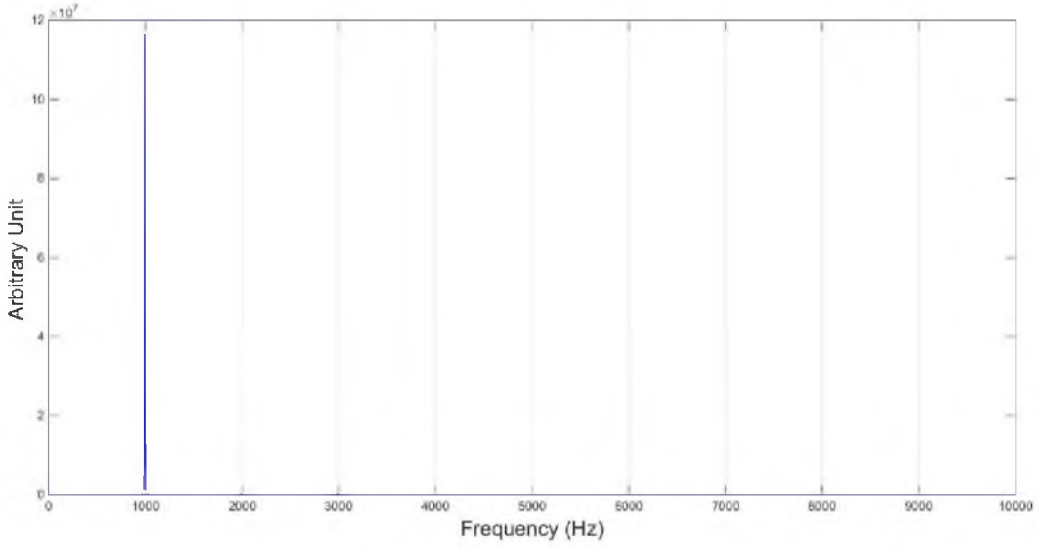

Figure 5.45 Filtered FFT analysis at 1000 Hz.

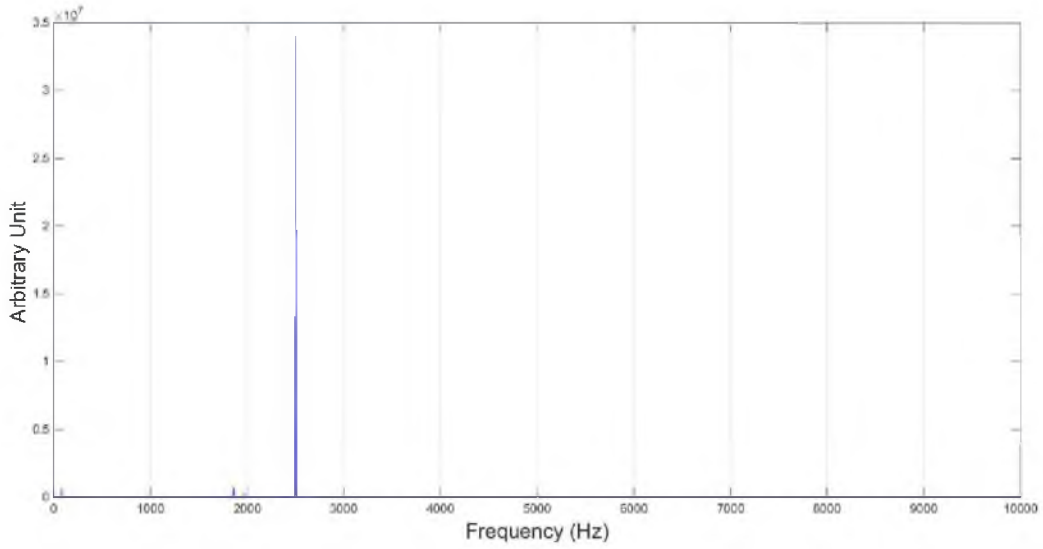

Figure 5.46 Filtered FFT analysis at 2.5 kHz.

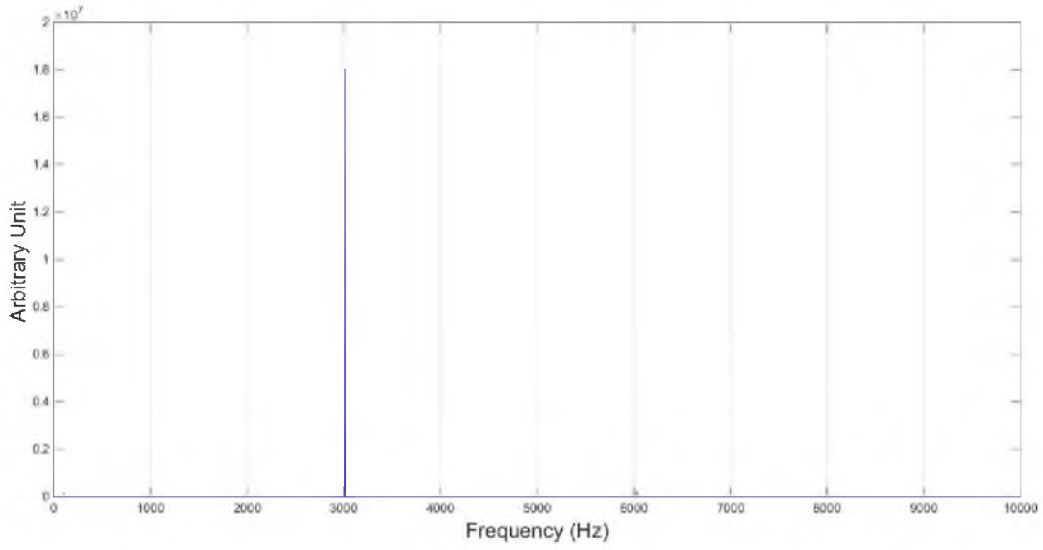

Figure 5.47 Filtered FFT analysis at 3 kHz.

$$F_o = \frac{\alpha . t}{L^2}$$

where α is a thermal diffusivity

t is a characteristic time

L is a characteristic length

Based on Rahman's study, the characteristic length between two parallel steel wool filaments is 0.0000541 m [8]. This length was used in Fourier number calculation.

And $\alpha = \frac{K}{\rho . Cp}$

where k=thermal conductivity of air at 300 k = 0.0263 W/m .k

ρ = density of air at 300 k = 1.16 kg/m^3

Cp = constant pressure - specific heat of air at 300 k = 1.007 kJ/kg.k

At 1000 Hz, t = 1/1000, therefore F_o = 7.5 at 1000 Hz.

Based on the equation of the penetration depth of surface temperature fluctuation [8], and the Fourier's equation, the relationship between the penetration depth (δ) and the average distance between two steel wool filaments (L) is $F_o = (\frac{\delta}{L})^2$, therefore the penetration depth is δ = 0.00147 m at 1kHz.

For frequencies less than 1 kHz, δ is much greater than L. In this case, the air trapped in the steel wool was strongly affected by steel wool temperature fluctuation. For frequencies above 1 kHz, δ becomes closer and maybe smaller than L, indicating some air in the steel wool was not affected by steel wool temperature change. This might explain the change in slope of the sound amplitude curve in Figure 5.33.

Figure 5.35 shows that the amplitude of the filtered thermoacoustic signal at 241 Hz shown in Figure 5.22 was reduced from 5.17 V (98.3 dB) to 5.15 V (98.1dB) after applying a high pass filter with a cut off frequency equal to 70 Hz. Applying a low pass filter with a cut off frequency of 300 Hz removed the short peaks in Figure 5.41 which were generated when the sine wave truncated. The effect of applying a high pass filter to the microphone signals for other frequencies can be seen in the wave forms in Figures 5.36 to 5.39. These signals showed less variation in maximum amplitude, but the RMS amplitude decreased slightly after filtering. Filtered FFT plots in Figures 5.44 to 5.47 show little difference from the unfiltered plots, indicating the generated sound waves are almost sinusoidal waves.

Details about the specifications of the MATLAB filter can be found in Appendix C.

5.2.4 Comparison of Data Before and After Noise Reduction Techniques

Figure 5.48 shows two sets of data collected at different times (summer 2014 and spring 2015) in order to show the change in thermoacoustic signal amplitude before and after noise reduction techniques and due to the improvement in air tightness.

The first set of data (before noise reduction technique) was collected during summer 2014. It shows that the amplitude of thermoacoustic signal starts to decrease with frequency in the low-frequency range and then approaches an almost constant value at high frequencies. The second data set (after noise reduction technique) was collected during spring 2015, and demonstrates the amplitude of thermoacoustic signals decreased nearly linearly with increasing the speed of the chopper wheel. The amplitude of the

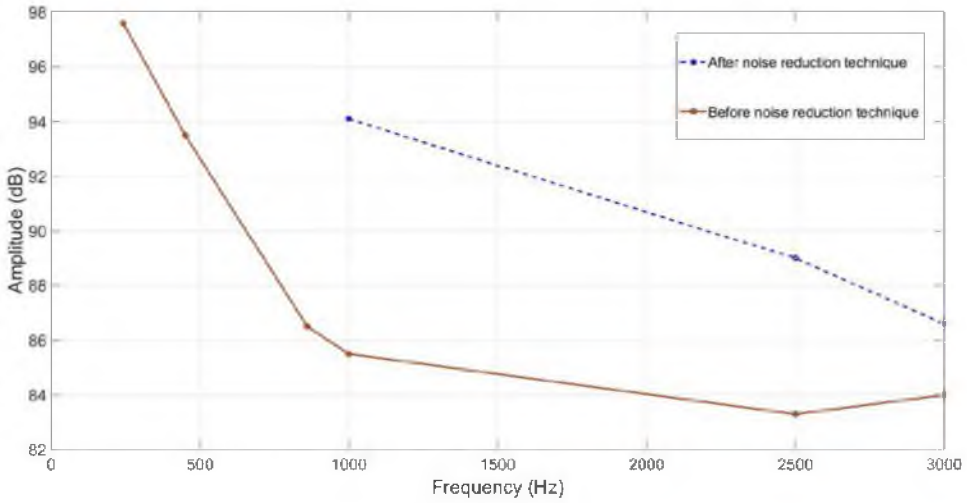

Figure 5.48 Two sets of data for thermoacoustic signals collected during the outdoor experiment.

thermoacoustic signal recorded in 2015 is higher than the amplitude of the TA signal collected in 2014 and is also clearer and purer. The improvement of the amplitude of the TA signal and the reduction of the background noise in 2015 could be attributed to the better airtight design, and the use of a shock mount device, new electric connections, and insulation materials. Figure 5.48 shows the percentage difference was 60% in the kHz frequency range.

5.3 Uncertainty Analysis

An uncertainty analysis was performed to achieve a level of confidence in the present experimental results. To assess the repeatability of the TA data measurements, Aowabin Rahman, a graduate student at the University of Utah, repeated the outdoor experiment with the same conditions, including the alignment of the TA system, solar flux, sound measurements, and the time of the experiment. Compared with Rahman's

high-frequency data which were collected in March 2015, there was only a small difference between his and the author's measurements collected on different dates, as shown in Figure 5.49. The difference in sound amplitude measurements was about 0.3 V for most frequencies. The small error in repeatability has little effect on the experiment results except for those at very high frequencies.

A method described by Kline and McClintock was used in this experiment to estimate the possible value that error might have in experiment measurements [54]. Based on a 95% confidence level, the author estimated the uncertainty for various parameters (length, voltage, and angle) in this experiment.

Uncertainty measurements for the devices used in this experiment (sound pressure level, multimeter, and pyranometer) were specified by the devices' manufacturers. The uncertainties of these devices were: $\pm$ **1.5** dB for the SPL device, $\pm$ **1%** $\pm$**2*D*** at 2000 mV for the multimeter, and $\pm$ **5%** for the pyranometer. The estimation of the uncertainty of the length measurements was 0.002 m, and the uncertainty of the angle measurements in the calibration process is 2°.

Furthermore, the error introduced in the use of microphone universal calibration curve is about 3–5 dB, as illustrated in Appendix D.

5.4 Conversion Efficiency of the TA Converter

In order to determine the conversion efficiency of the TA system studied in this thesis, we need to determine the acoustic energy generated by the converter and solar energy in the TA conversion system. The conversion efficiency formula is: efficiency is equal to acoustic energy generated divided by solar energy input. The acoustic energy

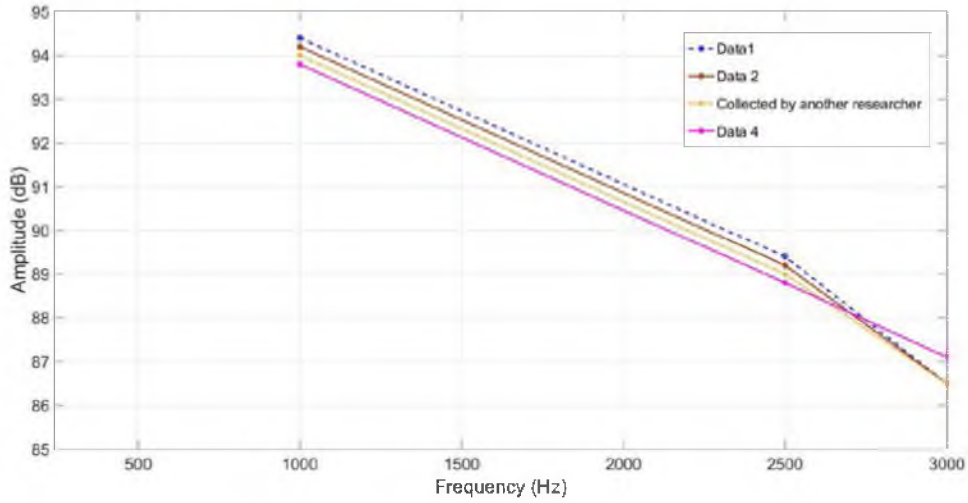

Figure 5.49 Comparison of the data for the outdoor experiment under the same working conditions to reproduce the thermoacoustic signal.

density of a point source can be calculated using equation 5.1. [55]

$$I = I_0 \times 10 \wedge \frac{(LI)}{I0} \tag{5.1}$$

where L_I = sound level in dB.

$I_0 = 10^{-12}$ watt/m^2 = reference intensity.

Using data from Appendix D, the sound intensity at 1000 Hz was: I = .001023292 watt/m^2.

The microphone area can be calculated using equation 5.2:

$$\text{Am} = \pi(R_m)^2 \tag{5.2}$$

where R_m = 0.0025m.

Thus, the acoustic energy received by the microphone was approximately (the sound waves can be approximated as planar waves) 0.00000002 watt at 1000 Hz.

The solar flux was 1025 w/m^2 with lens area calculated using equation 5.3:

$$A = \pi r^2 \tag{5.3}$$

where r= 0.365 m.

Therefore the solar energy input was 429 watts and the conversion efficiency was $4.6835 \times 10^{\wedge -11}$.

The above efficiency is underestimated since the surface area of the TA converter interior is much greater than the microphone surface area. In addition, the rate of solar energy that entered the converter was much less than the rate of solar radiation incident on the lens.

Moreover, power consumed by the electric motor in this experiment was measured by using a clamp meter to determine the exact current. The power formula below was used to calculate the consumed electric motor power:

Power= voltage × current

The power was 132–139.3 watt at 50.33 RPS.

The current for each wire of the three-phase motor was measured individually by using a clamp meter.

The current was measured at different speeds of the chopper wheel, as shown in Table 5.3.

Multiple TA converters can share one chopper wheel. In this case, the electricity consumption rate per TA converter would be much less. In addition, the chopper wheel can be placed inside a transparent vacuum chamber to reduce the amount of consumed electric power.

Table 5.3 The motor currents at different chopper-wheel-rotational speeds.

Speed of the chopper wheel (RPS)	**Current (Ampere)**
4	0.1
16.66	0.7–0.8
41.88	2–2.1
50.33	1.8–1.9

CHAPTER 6

CONCLUSION

This study examined the performance and efficiency of an improved thermoacoustic energy converter and the influences of various noises on the thermoacoustic signals generated by pulsed thermal radiation.

A shock mount device, insulation materials, and a new set of electric connection cables were used in this experiment to produce clearer thermoacoustic signals with high amplitude. Glass tinting films were used to reduce the solar intensity in order to alleviate microphone signal distortions in the low-frequency range (241–860 Hz).

By applying noise reduction techniques on the converter and the test stand, noise was reduced by 93%. The converter that was more airtight showed a 274% increase in sound amplitude at 241 Hz when compared with previous studies of similar TA converters. Experimental results with different intensities of solar flux showed a linear relationship between the sound amplitude and the frequency of the pulsed radiation beam for pulsed frequencies higher than 1000 Hz. In the low-frequency range, this relationship was more exponential than linear.

APPENDIX A

EQUIPMENT SPECIFICATIONS

Table A.1 Specifications of electric motor (Dayton company) [56]:

Feature	Electric motor (2nKY4)
Power rate	1.5 HP (General purposes)
Maximum rotational speed	3490
Phase type	three
Voltage rate	(208–230 V)
Full load Ampere	(4.5–4.1 A)

Table A.2 Specifications of sound pressure level (SPL) (72-942**)** [47]:

Feature	Sound pressure level (SPL) (72–942)
Frequency range	31.5Hz–8KHz
Measuring level range	30.0–130dB
Microphone	1/2 inch condenser microphone
Time weighting	FAST (125mS), SLOW (1 sec.)
Level ranges	Lo: 30–100dB, Hi: 60–130dB
Accuracy	± 1.5dB
Power supply	One 9V battery
Dimension	8-1/4" (L) × 2-1/4" (W) × 1-1/4" (D)

Table A.3 Specifications of the pyranometer [57]:

Feature	Pyranometer/Apogee company
Sensitivity	0.20 mV per W m-2
Calibration Factor	5.0 W m-2 per mV (reciprocal of sensitivity)
Calibration Uncertainty	± 5 %.
Non-stability (Long-term Drift)	< 2 % per year
Response Time	< 1 Ms
Temperature Response	-0.04 ± 0.04 % per C
Operating Environment	-40 to 70 C 0 to 100 % relative humidity can be submerged in water up to depths of 30 m
Dimensions	2.40 cm diameter and 2.75 cm height
Mass	90 g (with 5 m of lead wire).
full scale output	200 mV

Table A.4 Specification of the data acquisition card (NI USB 6009) [44]:

Feature	Data acquisition card (NI USB 6009)
Number of Input analog ports	Eight channels (12 bit)
Number of Output analog ports	Two channels (12 bit)
Number of Input, Output analog ports	Twelve channels (32 bit), Twelve channels (32 bit)
Maximum AI sample rate, single channel*	48 kS/s
Maximum AI sample rate, multiple channels (aggregate)*	48 kS/s
AI resolution	14 bits differential, 13 bits single-ended
DIO configuration	Open collector or active drive

*System-dependent

Table A.5 Generator specifications [58]:

Feature	Generator/Chicago electric company
Fuel Capacity	4 Gallons of unleaded gasoline
Engine type	4 Stroke with 7 HP
Electrical plugs	20 A Duplex NEMA 120 V Receptacle. 25 A NEMA 120 V Twist lock Receptacle 10 A DC Breaker.
SPEED	3600 RPM
Power	3050 Watt

Table A.6 Multimeter (model number 98025) specifications [59]:

Feature	Multimeter
Power requirement	9V
Frequency	45 to 450 Hz
Accuracy	@200 mV % 0.5 @2000 mV % 1
Resistance	Range:200/2000/20K/200K,2000K ohm
Dc Voltage	Range:200 mV/2000mV 20/200,2000 V

APPENDIX B

ENGINEERING DRAWING OF TA CONVERTER

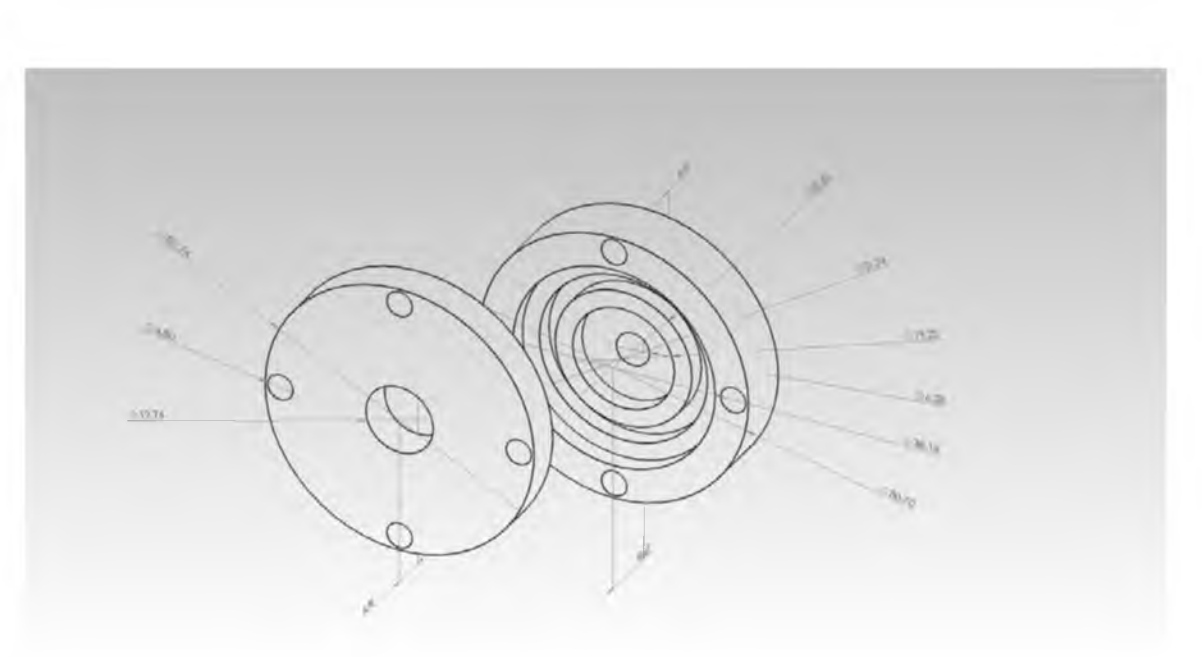

Figure B.1 The dimensions of the TA converter.

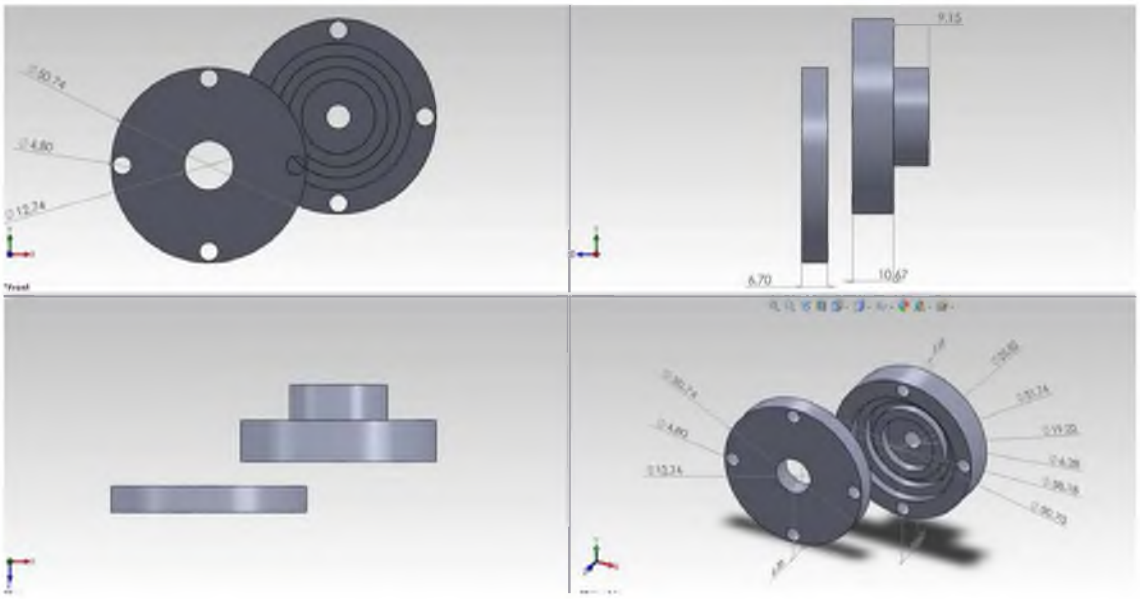

Figure B.2 Three views of the converter (top, front, and side) and the isometric view.

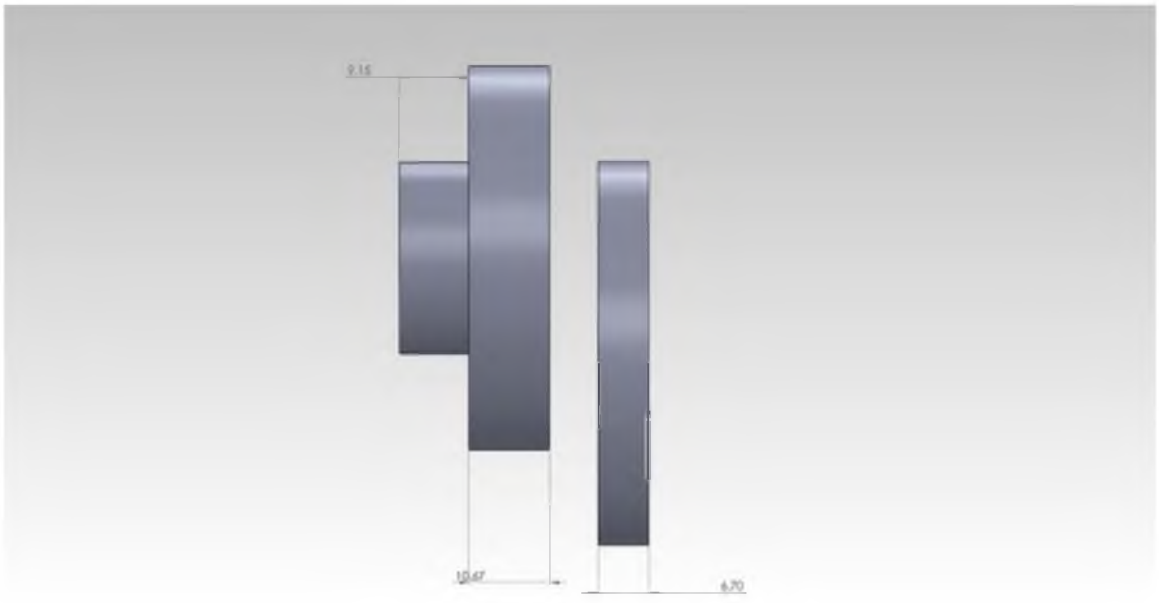

Figure B.3 Side view of the TA converter

APPENDIX C

SOFTWARE FOR TA SIGNAL ANALYSIS

The procedure to run the LabVIEW software is outlined below:

1. Launch the LabVIEW software. Choose the "Add step" option from project view. Select "Acquire signal" and then "Analog." Last, choose "Voltage." This step was used to determine the sampling number and rate for the signal. The sampling number in this study was 5 kHz and the sampling rate was 20 kHz for all collected data. The time period in this study was 0.25 second.
2. Select "Add step" option. Select "Time domain measurement" and then "Amplitude and level." (Root Mean Square (RMS) peak to peak value can be determined in this step.)
3. Select "Add step" option. Select "Frequency domain measurement" and then "Frequency and Total Harmonic Distortion (THD)." Frequency and THD can be specified by using this option. Then right click on the screen to select which signal to do the analysis on. Select Voltage signal. Press Run button on tools bar.

Shown below is the MATLAB code developed to plot the digitized TA signals in time domain and to perform FFT of the time-domain data.

```
clc,clear
```

```
data=load('File name.csv')
plot(data(:,1),data(:,2),'-b')
xlabel('Time (Second)','FontSize', 24)
ylabel('Amplitude (Volt)','FontSize', 24)
set (gca,'fontsize',20)

clc,clear
data=load('File name.csv')
dhat = fft(data(:, 2));
freq = linspace(0, 1, size(data,1)/2) *20000/2;
power = dhat.*conj(dhat);
plot(freq,power(1:length(freq)))
xlabel('Frequency (Hz) ','FontSize', 24)
ylabel('Arbitrary unit','FontSize', 24)
set (gca,'fontsize',20)
```

Filter specification of the MATLAB software:

- Select low or high filter (response type) depending on type of the analysis.
- IIR (infinite impulse response)/Butterworth should be the design method (efficient and fast filter).
- Filter order is 2
- Sampling rate 20000 Hz.
- Cut off frequency 70 or 500 depending on the frequency.

APPENDIX D

CALIBRATION PLOTS FOR DIFFERENT FREQUENCIES

AND A UNIVERSAL PLOT

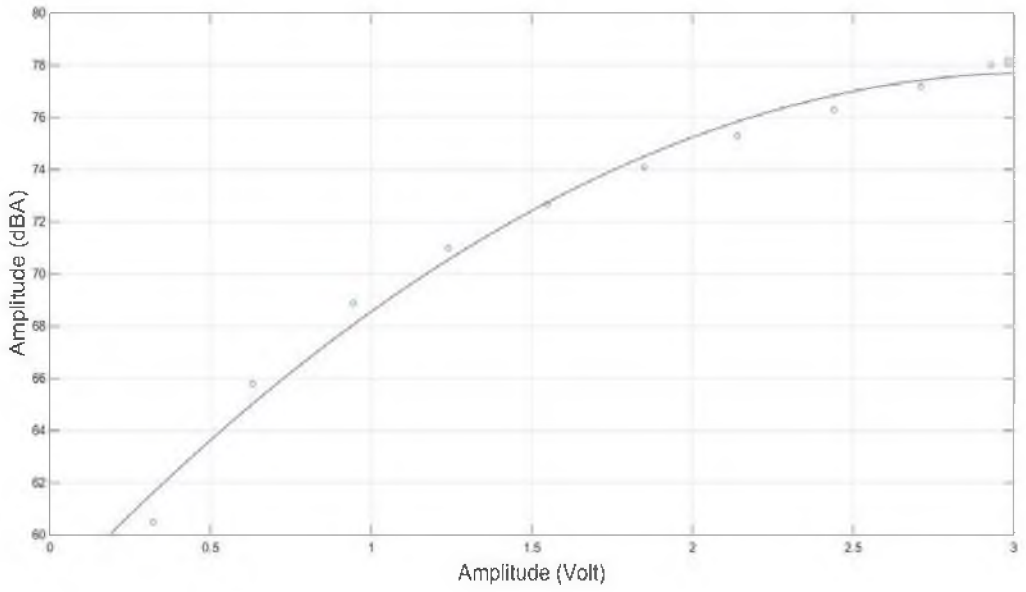

Figure D.1 Calibration plot at 100 Hz frequency.

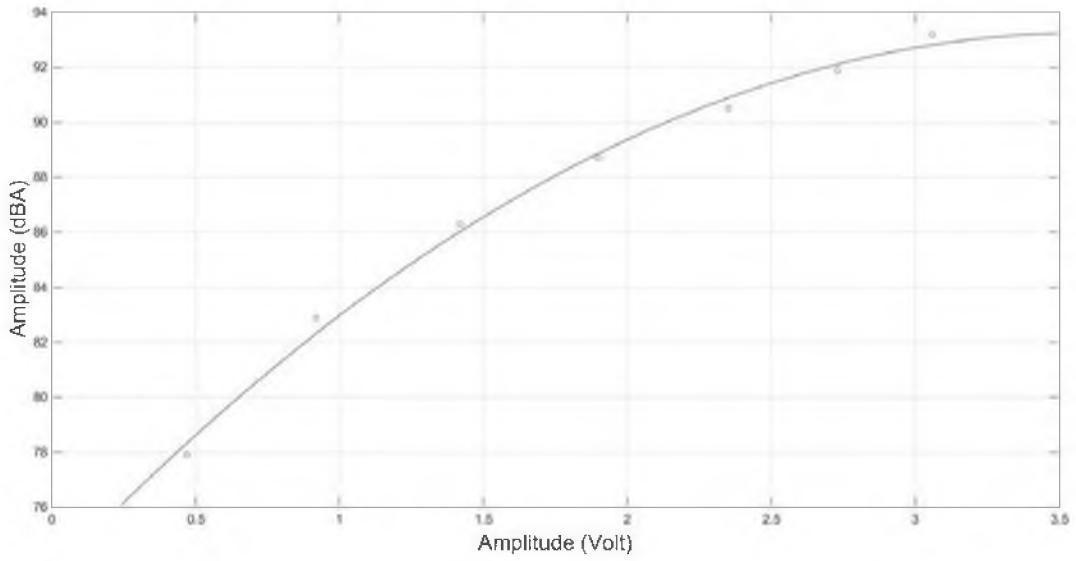

Figure D.2 Calibration plot at 400 Hz frequency.

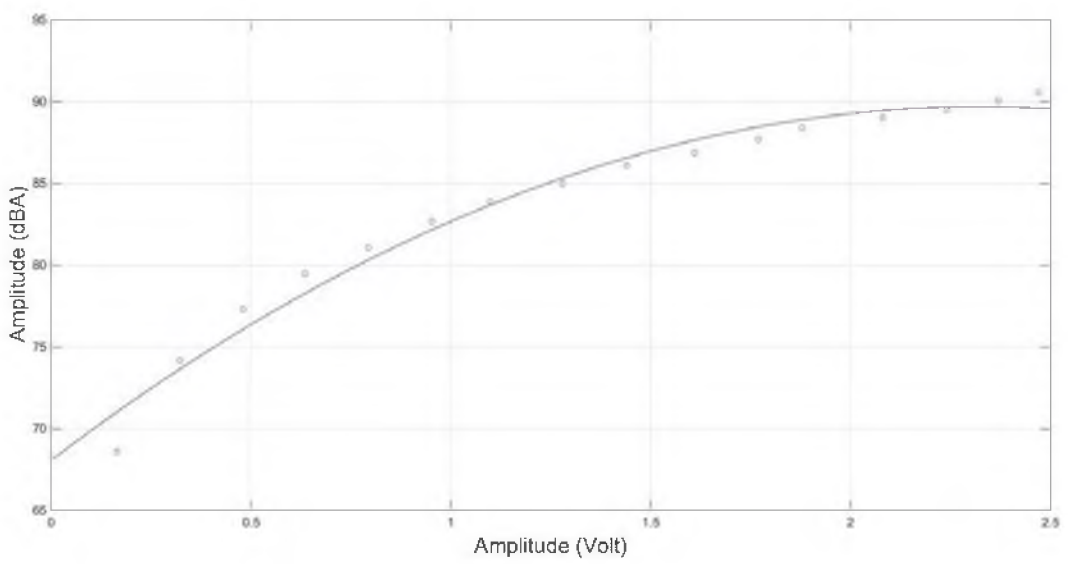

Figure D.3 Calibration plot at 1000 Hz frequency.

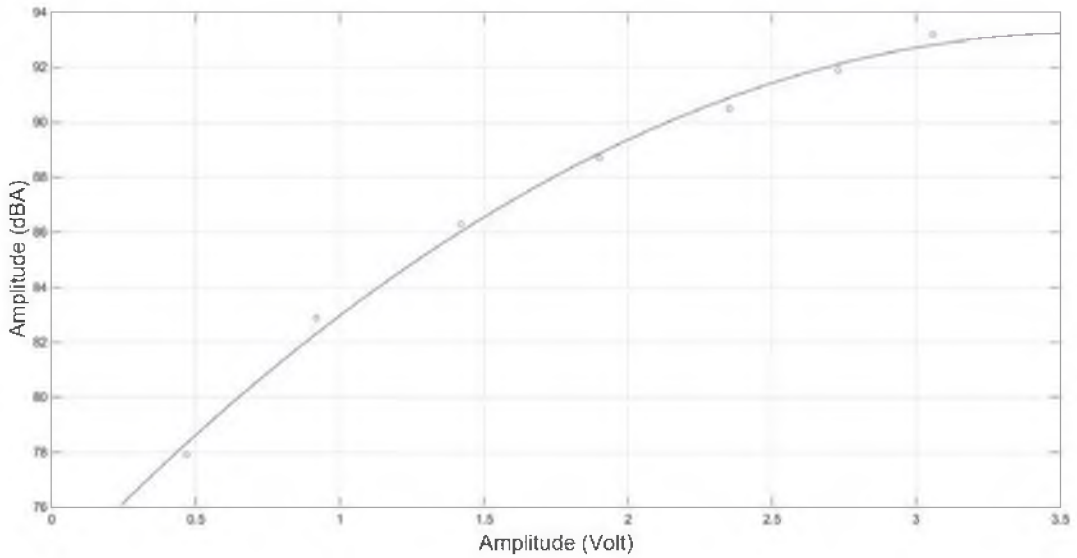

Figure D.4 Calibration plot at 3000 Hz frequency.

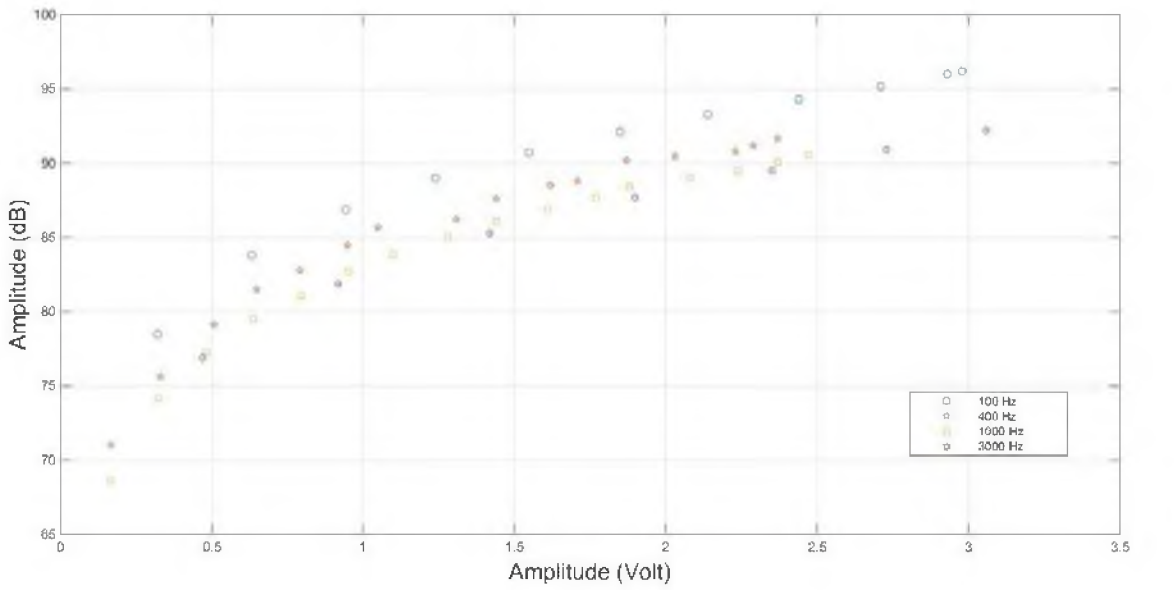

Figure D.5 Microphone calibration data collected in the present study.

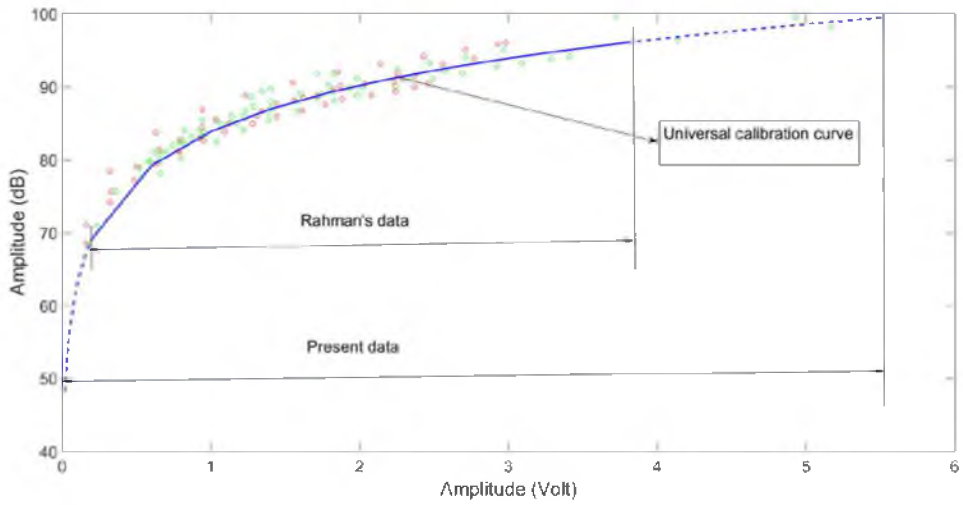

Figure D.6 Microphone calibration data collected in this study and in Rahman's thesis study and microphone universal calibration (microphone calibration curve was based upon data from (0.2–3.8 V)) [8].

APPENDIX E

EXPANDED TIME DOMAIN SIGNALS

The time domain signals (voltage signals) below were expanded at 100 and 3000 Hz for data collected during the indoor experiment to show if the signals were truncated.

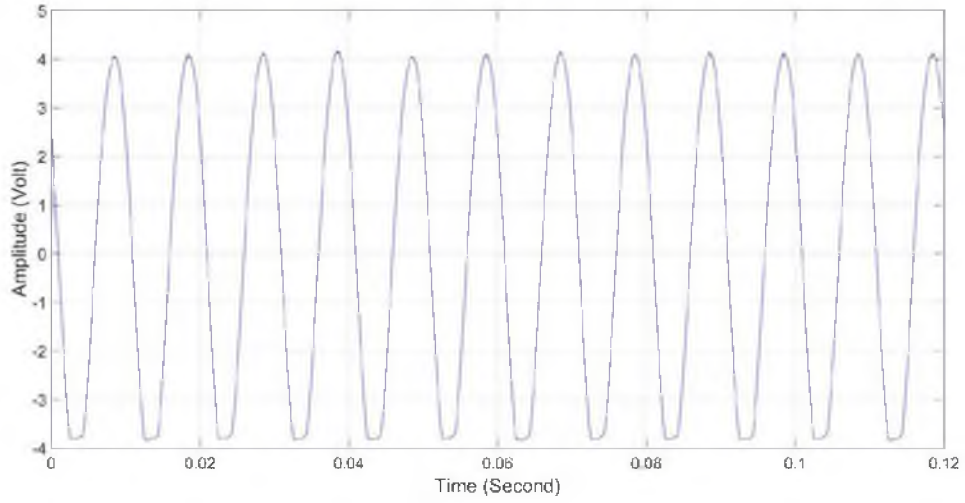

Figure E.1 The amplitude of signal (RMS) is 2.96 V (or 96.2 dB) at 100 Hz to show clearly the truncation after expanding the signal.

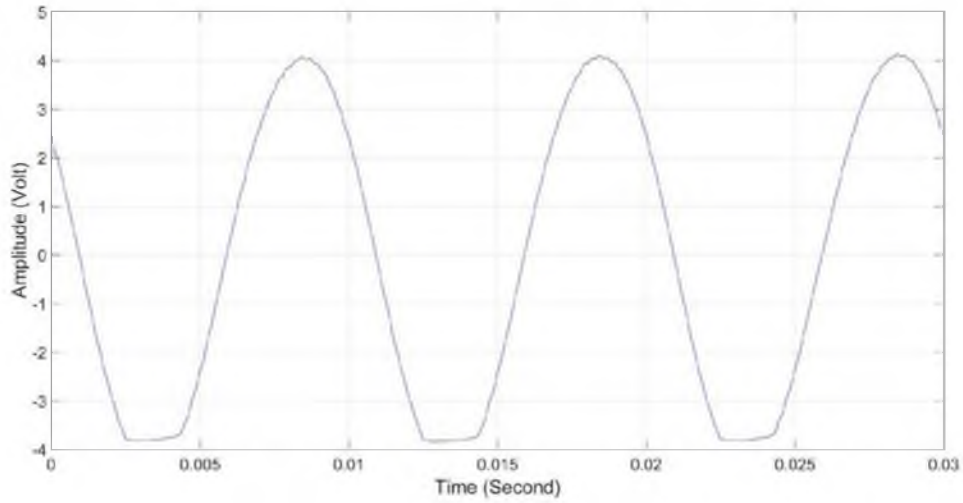

Figure E.2 Expanding Figure E.1.

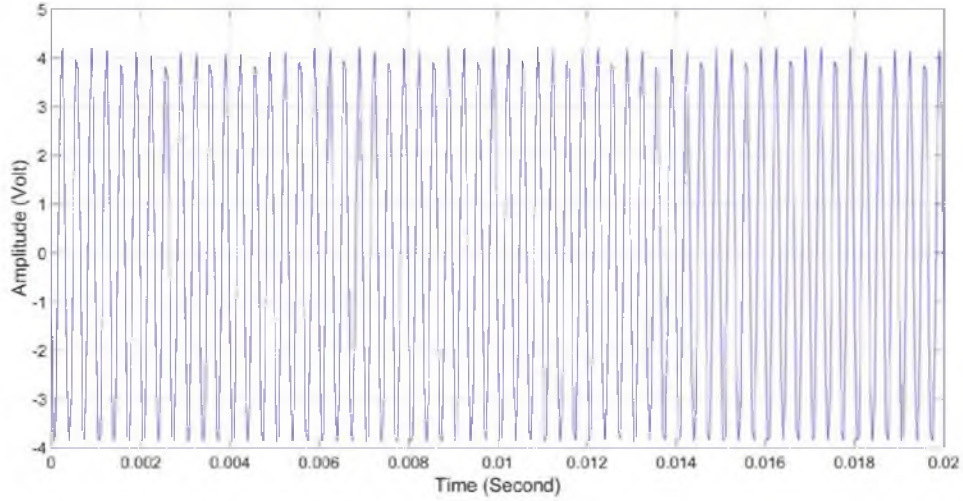

Figure E.3 The amplitude of signal (RMS) is 3.04 V (or 92.5 dB)
at 3000 Hz to show clearly the truncation
after expanding the signal.

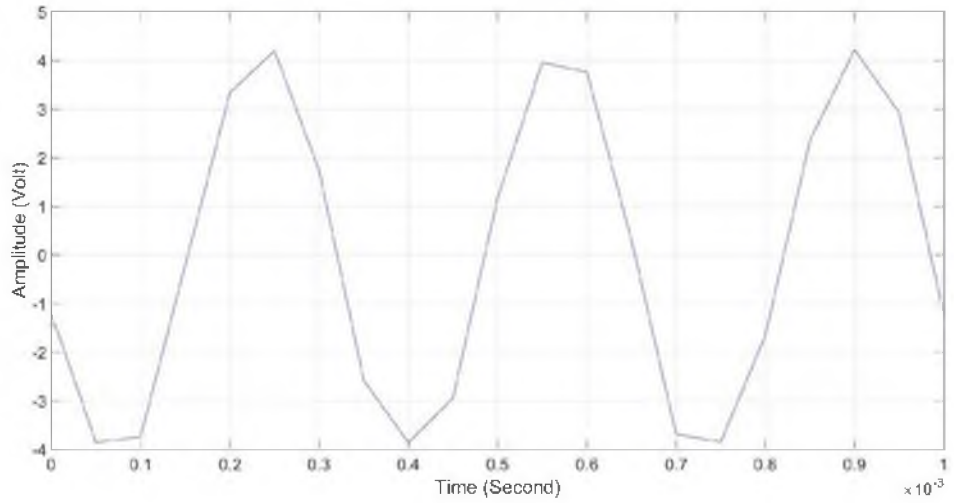

E.4 Expanding Figure E.3.

REFERENCES

[1] H. Babaei and K. Siddiqui, "Design and optimization of thermoacoustic devices," *Energy Conversion and Management,* vol. 49, pp. 3585-3598, 2008.

[2] C. L. Morfey, *Dictionary of Acoustics*. San Diego, CA: Academic Press, 2001.

[3] D. Fahey, "Thermoacoustic oscillations," unpublished.

[4] J. B. S, A. K. R, and S. V. S, "Study on a standing wave thermo acoustic refrigerator made of readily available materials," *International Journal of Scientific and Research Publications (IJSRP),* vol. 3, pp. 30, 2013.

[5] M. P. Norton and D. G. Karczub, *Fundamentals of Noise and Vibration Analysis for Engineers*. Cambridge, United Kingdom: University of Cambridge, 2003.

[6] C. E. Speaks, *Introduction to Sound; Acoustics for the Hearing and Speech Sciences*, 2nd ed. San Diego, CA: Singular Pub., 1996.

[7] G. Huelsz and E. Ramos, "An experimental verification of Rayleigh's interpretation of the Sondhauss tube," *Journal of the Acoustical Society of America,* vol. 106, pp. 1789-1793, 1999.

[8] A. Rahman, "Generation of thermo-acoustic waves from pulsed solar/IR radiation," M.S. thesis, Mechanical Engineering, Univ. of Utah, Salt Lake City, UT, 2014.

[9] N. H. M. Abd Settar, "Thermal performance of a thermoacoustic stack," M.S. thesis, University Teknologi Malaysia, Johor Bahru, Malaysia, 2008.

[10] D. L. Hutt, K. J. Snell, and P. A. Bélanger, "Alexander Graham Bell's photophone," *Optics and Photonics News,* vol. 4, pp. 20-25, 1993.

[11] K. Chen *et al.*, "Acoustic energy output and coupling effect of a pair of thermoacoustic lasers," *International Journal of Energy Research,* vol. 36, pp. 477-485, 2012.

[12] A. Badiger, "A project on thermoacoustics," Online slideshow, internet: http://www.slideshare.net/aravindbadiger7/project-a-thermoacoustics-20650148, 2013.

[13] (2015, July 1). *Primasonics*. [Online]. Available: http://www.primasonics.com/applications

[14] A. S. L. H. Association. (1997-2015). *Practice Portal: Hearing Loss - Beyond Early Childhood*. [Online]. Available: http://www.asha.org/Practice-Portal/Clinical-Topics/Hearing-Loss/

[15] Dolcera. (2012). *Ultrasonic food processing-baking*. Available: http://www.dolcera.com/website_prod/ultrasonic-food-processing-baking

[16] G. Huan *et al.*, "Nonlinear impedances of thermoacoustic stacks with ordered and disordered structures," *Chinese Physics B,* vol. 23, pp. 074301, 2014.

[17] X. Mao, "Study of fluid flow phenomena around parallel-plate stacks in a standing wave thermoacoustic device," Ph.D. dissertation, School of Mechanical, Aerospace and Civil Engineering, University of Manchester, Manchester, United Kingdom, 2011.

[18] F. Saunders, "A sound use for heat," *American Scientist Online,* vol. 95, pp. 491, December, 2007.

[19] R. Surathu, "A study of coupling two thermoacoustic lasers," M.S. thesis, Mechanical Engineering, Univ. of Utah, Salt Lake City, UT, 2013.

[20] A. Rosencwaig and A. Gersho, "Theory of the photoacoustic effect with solids," *Journal of Applied Physics,* vol. 47, pp. 64-69, 1976.

[21] S. R. Timothy, "Design and control of a standing-wave thermoacoustic refrigerator," M.S. thesis, Mechanical Engineering, University of Pittsburgh, Pittsburgh, PA, 2009.

[22] C. Dip. (2015, February 15) *Bell photophone* [Online]. Available: https://www.youtube.com/watch?v=YNlyEpRXX7o, 11 Jun 2015

[23] D. Slater, "Passive long range acousto-optic sensor," in *Proceedings of SPIE - The International Society for Optical Engineering*, 2006.

[24] A. G. Bell, "LXVIII. Upon the production of sound by radiant energy," *The London, Edinburgh, and Dublin Philosophical Magazine and Journal of Science,* vol. 11, pp. 510-528, 1881.

[25] F. M. MIMS III, "Alexander Graham Bell and the photophone: the centennial of the invention of light-wave communications, 1880–1980," *Optics News,* vol. 6, pp. 8-16, 1980.

[26] F. J. Harren *et al.*, "Photoacoustic spectroscopy in trace gas monitoring," *Encyclopedia of Analytical Chemistry,* 2000, pp. 2.

[27] J. W. S. Rayleigh, *The Theory of Sound*, 2nd ed., rev. and enl. ed. London, United Kingdom: Macmillan and Co., 1896, pp. 226.

[28] I. Johney, "Photo acoustic investigation in phase transitions in selected solids," Ph.D. dissertation, Department of Physics, Cochin University of Science and Technology, Kochi, India, 1991.

[29] E. Xavier, "Studies on electrical and thermal properties of certain selected photonic materials," Ph.D. dissertation, International School of Photonics, Cochin University of Science and Technology, Kochi, India, 1997.

[30] H. Babaei and K. Siddiqui, "Design and optimization of thermoacoustic devices," *Energy Conversion and Management,* vol. 49, pp. 3585-3598, 2008.

[31] L. Zoontjens *et al.*, "Feasibility study of an automotive thermoacoustic refrigerator," in *Annual Conference of the Australian Acoustical Society 2005, Acoustics 2005: Acoustics in a Changing Environment*, 2005, pp. 299-307.

[32] S. A. Kolhe, "An experimental investigation of thermoacoustic lasers operating in audible frequency range," M.S. thesis, Mechanical Engineering, Univ. of Utah, Salt Lake City, UT, 2012.

[33] M. W. Sigrist, "Laser generation of acoustic waves in liquids and gases," *Journal of Applied Physics,* vol. 60, pp. R83-R122, 1986.

[34] N. M. Ghazali. "Thermoacoustic heat engine," *Jurnal Teknologi*, vol. 40(1), pp. 67-78, June 2004.

[35] s. parts. (2014). *325 Silicone O-Ring, 70A Durometer, Red, 1-1/2" ID, 1-7/8" OD, 3/16" Width (Pack of 5)*. [Online]. Available: http://www.amazon.com/325-Silicone-O-Ring-Durometer-Width/dp/B000FN0Y8K/ref=sr_1_1?ie=UTF8&qid=1435261738&sr=8-1&keywords=silicon+o+ring&pebp=1435261749314&perid=1C7S1DP9G5DA5GMD3EP8]

[36] C. Hopkins, *Sound Insulation*. Burlington, MA: Elsevier, 2007.

[37] J. Conrad and J. Hemond, *Engineering Acoustic & Noise Control*. Englewood Cliffs, NJ: Prentice Hall, 1983.

[38] Home Depot, http://www.homedepot.com/l/21st-South/UT/Salt-Lake-City/84115/4403.

[39] I. Acoustics by Design. (2009, January 29). *Absorbing Vs. Blocking Sound.* [Online]. Available: http://www.acousticsbydesign.com/acoustics-blog/absorbing-vs-blocking-sound.htm

[40] Pellor.Best.Deals, New Universal 50mm Microphone Shock Mount for 48mm-54mm Diameter Condenser Mic. [Online] Available: http://www.ebay.com/itm/New-Universal-50mm-Microphone-Shock-Mount-for-48mm-54mm-Diameter-Condenser-Mic-/151501590432?ssPageName=ADME:X:AAQ:US:1123

[41] Q-see, Q-See 50FT BNC Video & Power Cable with 2 Female Connectors. [Online]. Available: http://www.amazon.com/Q-See-Video-Power-Female-Connectors/dp/B001CIREDU/ref=sr_1_sc_1?ie=UTF8&qid=1421188411&sr=8-1-spell&keywords=q+see+50+ft+bnc+vide

[42] Dimart, Dimart BNC Male to Dual 4mm Banana Plug Oscilloscope Test Lead Cable 3.5ft. [Online]. Available: http://www.amazon.com/Dimart-Banana-Oscilloscope-Cable-3-5ft/dp/B00PFBDE34/ref=sr_1_2?ie=UTF8&qid=1421189010&sr=8-2&keywords=dimart+bnc+male

[43] Videosecu, VideoSecu High Sensitive Audio Pickup Device External Amplified Tiny Spy Microphone for CCTV Security Camera with Bonus Warning Decal WD6. [Online]. Available: http://www.amazon.com/VideoSecu-Sensitive-External-Amplified-Microphone/dp/B0053V5Z9W/ref=sr_1_1?ie=UTF8&qid=1417633493&sr=8-1&keywords=video+spy+microphone

[44] National Instruments Austin City, TX, USA *Data* Data Acquisition Card, *Model 6009* (2012) [Online]. Available: http://www.ni.com/pdf/manuals/371303m.pdf [Apr. 29, 2015].

[45] W. Tint. (2013). *Pro High Performance 70% VLT Auto Window Tinting Film 30 Inch Wide x 10 Feet Long Roll.* [Online]. Available: http://www.amazon.com/High-Performance-Auto-Window-Tinting/dp/B00F8PQ1M8/ref=sr_1_2?ie=UTF8&qid=1432012333&sr=8-2&keywords=windows+tint+VLt+70%25

[46] N. software. *Tone generator software*. [Online]. Available: http://www.nch.com.au/tonegen/index.html

[47] Premier Farnell Chicago, IL, USA. (2015, April 29). *Sound Pressure Level, Model* 72-942 (2012). [Online]. Available: http://www.farnell.com/datasheets/1537621.pdf

[48] A. Asplund, "How loud was it? A calibration system for voice recording in clinical and research applications," in *Proceedings of the 26th World Congress of Logopedics and Phoniatrics*, 2004.

[49] R. Tipton. (2009). DIY microphone calibration. *audioXpress*. 1-4. [Online]. Available: http://www.tdl-tech.com/miccalax.pdf

[50] M. Huckvale. (2003). *Acoustics of speech and hearing; Lecture 1-2 sound pressure level scale*. [Online]. Available: http://www.phon.ucl.ac.uk/courses/spsci/acoustics/week1-2.pdf

[51] P. Piezotronics. (2013). *Microphone handbook*. [Online]. Available: http://www.pcb.com/linked_documents/vibration/microphone_handbook.pdf

[52] A. C. Monteith and C. F. Wagner, *Electrical Transmission and Distribution Reference Book*, 4th ed. East Pittsburgh, PA: Westinghouse Electric Corporation, 1950.

[53] F. P. Incropera and D. P. DeWitt, *Fundamentals of Heat and Mass Transfer*, 4th ed. New York: John Wiley & Sons, 1996.

[54] S. J. Kline and F. McClintock, "Describing uncertainties in single-sample experiments," *Mechanical Engineering,* vol. 75, pp. 3-8, 1953.

[55] (2015, July 16). *Conversion of sound units (levels)*. [Online]. Available: http://www.sengpielaudio.com/calculator-soundlevel.htm

[56] W.W Grainger, Inc, UT, USA. (2015, May 1). *electric motor, Model 2nKY4* (2013) [Online]. Available: http://www.grainger.com/product/DAYTON-GP-Mtr-2NKY4?nls=1&searchQuery=2nKY4

[57] A. Instruments. (2012, January 11). *Pyranometers*. [Online]. Available: http://www.apogeeinstruments.com/pyranometer/

[58] Harbor Freight Tools, UT, USA. (2015, May 1). *Chicago Electric Generator, Model 67560* (2015). [Online]. Available: http://images.harborfreight.com/manuals/67000-67999/67560.pdf

[59] Harbor Freight Tools, UT, USA. (2015, July 28). *Cen-Tech Seven Function Multimeter Model 98025 (2015)*. [Online]. Available: http://manuals.harborfreight.com/manuals/98000-98999/98025.pdf